Experimental response of a scaled dry-joint masonry arch subject to inclined support displacements

Chiara Ferrero[a,b*], Chiara Calderini[a], Pere Roca[b]

[a]*Department of Civil, Chemical and Environmental Engineering, University of Genoa, Via Montallegro 1, 16145 Genoa, Italy*

[b]*Department of Civil and Environmental Engineering, Technical University of Catalonia (UPC-BarcelonaTech), Jordi Girona 1-3, 08034 Barcelona, Spain*

* corresponding author

E-mail addresses: chiara.ferrero@edu.unige.it (Chiara Ferrero), chiara.calderini@unige.it (Chiara Calderini), pere.roca.fabregat@upc.edu (Pere Roca).

Experimental response of a scaled dry-joint masonry arch subject to inclined support displacements

Abstract: Support displacements are a major cause of damage to masonry arches. In the last decades, the effect of large support displacements on the stability of masonry arches has been widely investigated. However, there is still a lack of studies dealing with inclined support displacements. In this work, a large experimental campaign was performed on a 1:10 small-scale segmental masonry arch subjected to several combinations of vertical and horizontal support displacements. The mockup was built as a dry-joint assemblage of blocks and was tested to collapse by using an ad hoc designed testing machine. The effects of the displacement direction on the arch static behaviour were evaluated in terms of evolution of the hinge configuration, collapse mechanism, support reaction-displacement curves, ultimate displacement capacity and support reactions at collapse. In light of the experimental results, new conclusions about the arch response to inclined support displacements were drawn. A limit displacement domain, computed as a function of the direction of the imposed support displacements, was also proposed.

Keywords: dry-joint masonry arches; inclined support displacements; settlements; experimental tests.

1. Introduction

Masonry arches play a fundamental role in the static behaviour of historic masonry buildings. Consequently, their structural integrity is a crucial issue for the conservation of built cultural heritage. Masonry arches and, more in general, masonry structures are sensitive to any small change in the boundary conditions. As a result, support displacements are one of the primary sources of damage for masonry arches. The potential causes of support displacements are various, including foundation settlements, soil heterogeneity, leaning of supporting pillars, subsidence, and landslides. Although the movements originated from these phenomena are generally small in their instantaneous value, they can produce severe damage and even collapse if they increase significantly over time [1].

Considerable research effort has been made in the last two decades to assess the stability of masonry arches under large support displacements. Both experimental testing and computational methods were used for this purpose. This work only focuses on the experimental studies, while the reader is referred to [2] for a detailed review of the computational methods, most of which were validated through

comparison with experimental results (e.g., [1,3-17]). Note that experimental testing has been widely used in recent years to study the response to large support displacements not only of masonry arches but also of masonry vaults and domes (e.g., [18-26]).

Table 1 Experimental investigations on masonry arches subjected to support displacements.

Reference	Scale	Geometry	Span length [cm]	Voussoir material	Joints	Direction of support displacements (*)
[1,3]	Small-scale	Circular	39.0	Cast concrete	Dry joints	Horizontal (O)
		Segmental	70.9			
[5,6]	Small-scale	Circular	100.0	Cast concrete	Dry joints	Horizontal (O-I)/ vertical (U-D)
		Pointed				
[4]	Small-scale	Circular	30.0	Stainless steel	Dry joints	Horizontal (O)/ vertical
[27]	Small-scale	Pointed	140.0	Brick	Mortar joints	Horizontal (O)
		Parabolic				
[7-9]	Full-scale	Segmental	228.1	Brick	Mortar joints (with a plexiglass plate in the middle)	Vertical (D)/ inclined (45°, O)
[14]	Small-scale	Segmental	42.4÷53.5	PVC	Dry joints	Horizontal (O)/ vertical (D)
[15]	Small-scale	Pointed	30.0÷35.2	Autoclaved aerated concrete	Dry joints	Horizontal (O)
[10]	Small-scale	Segmental	62.0	Wood	Mortar joints	Horizontal (O)
[11]	Small-scale	Segmental	190.0	Brick	Mortar joints	Horizontal (O)
[12]	Small-scale	Segmental	53.0	Bicomponent composite material	Dry joints	Vertical (D)
[17]	Small-scale	Pointed	34.0÷36.8	Autoclaved aerated concrete	Dry joints	Vertical (D)

(*) I = inward; O = outward; U = upward; D = downward.

Table 1 summarizes the experimental studies carried out so far to investigate the structural behaviour of masonry arches on moving supports. Small-scale models found a wider application with respect to full-scale ones, which were built only in [7-9]. This is not surprising, as they are less expensive and faster to be assembled, do not require significant building skills, and allow one to repeat several trials for the same test. Furthermore, as described by Heyman in [28], when dealing with masonry constructions,

models at reduced scale can be confidently used to simulate full-scale structures since stability is a matter of geometry rather than material failure. For this reason, small-scale testing were recurrently used also in the case of masonry vaults on moving supports [18-20,23,24,29-32] as well as arches and vaults subjected to point loads [32,33]. Being the strength of the composing material irrelevant, a range of different materials, including concrete (cast or autoclaved aerated), stainless still, PVC, wood, and bricks, were used for the voussoirs of small-scale arches (see Table 1), which were assembled either with mortar or dry joints. It should be noted that only Alforno et al. [10] employed a voussoir size representing the scaled dimensions of real bricks.

The experimental tests carried out so far in the literature provided insight in the mechanics of masonry arches subjected to large support displacements, especially in the case of horizontal and vertical displacements, which were recurrently investigated (see Table 1). In contrast, the only reference for inclined displacements was the test performed on a full-scale segmental arch subjected to a support displacement inclined at 45° with respect to the vertical [7-9].

According to the experimental evidence, regardless of the arch geometry, three hinges initially appear when support displacements are imposed. As already observed in [9] and [14], the hinge position is strictly dependant on the direction of support displacements. In the case of horizontal and inclined (45°) support displacements, no matter the arch geometry, hinges alternate between the intrados and extrados (see [1,3-6,10,11,14,15,27]). In the case of vertical (downward) displacements, two consecutive hinges generally appear at the arch extrados on the side of the moving support (see [4-7,12,14]). However, in the case of pointed arches only, depending on the arch geometry and sharpness, hinges may also alternate between the intrados and extrados (see [5,6,17]). Several authors observed that hinges may change position with the increase of support displacements (e.g., [1,3-6]). In particular, the intrados hinges were often found to move towards the crown as the supports spread apart.

Once the three initial hinges have opened, as support displacements increase, the arch experiences progressive changes in the geometry which finally lead to collapse. In arches subjected to vertical and horizontal support displacements, collapse generally occurs when a fourth hinge appears. In the case of horizontal displacements (see [1,3,10] among others), this failure mode can be attributed to the slight asymmetry and geometrical imperfections of the physical models, since a perfectly symmetrical arch

would collapse by a symmetrical five-hinge mechanism [1]. In this regard, it should be noted that five hinges at collapse were observed only in [5,6]. A three-hinge snap-through failure was also found to occur in the case of horizontal spreading supports for arches with large thickness-to-radius ratios and small angles of embrace [5,6].

In the case of inclined support displacements, the only experimental test performed in the literature (see [8,9]) showed a collapse mechanism due to the alignment of the three initial hinges. However, it is likely that this failure mode was strictly related to the shape and geometry of the arch and, consequently, cannot be considered representative of the response of masonry arches to inclined support displacements.

In view of the foregoing, it is clear that further investigation on the effects of combined horizontal and vertical support displacements is needed, also considering that slow-moving landslides, which produce a combination of vertical and horizontal support displacements, were recently found to cause severe and extensive damage to the arches of historic masonry churches [34]. Furthermore, the few numerical investigations available in the literature on arches subjected to inclined support displacements showed that the direction of the imposed displacements can affect the arch response in terms of position of the three initial hinges [7,14,35] as well as collapse mechanism, ultimate displacement capacity and support reactions [35].

Taking this into account, this work aims at providing a full understanding of the mechanics of masonry arches subjected to inclined support displacements. For this purpose, a 1:10 small-scale model of a segmental arch was tested to collapse under several combinations of vertical and horizontal displacements of one support. The mockup was built as a dry-joint assemblage of blocks made of a bicomponent composite material. A testing machine was constructed ad hoc to perform the experimental tests, which took place in the Structural Engineering Laboratory of the University of Genoa. A new experimental set-up was also designed, which allowed the authors to measure not only the displacements of the arch voussoirs but also the reaction forces at the arch springings. The results from a preliminary test in which purely vertical support displacements were applied are reported in [12].

The main aim of this work is to experimentally evaluate to what extent the direction of the imposed support displacements influences the static behaviour of the tested arch in terms of evolution of the

hinge configuration, collapse mechanism, support reaction-displacement curves, ultimate displacement capacity and support reactions at collapse.

The present paper is organized as follows. In Section 2, the geometry, material and building process of the physical model are presented. In Section 3, the experimental set-up is described. In Section 4, the experimental results obtained when varying the direction of the support displacements are presented and critically discussed. In Section 0, some conclusions are drawn.

2. Physical model

The experimental tests were performed on a 1:10 small-scale model of a segmental dry-joint masonry arch supported by two piers (Fig. 1). The arch has an angle of embrace of 125°, a span length (L) of 533 mm, a rise of 162 mm and a radial thickness of 24 mm. As already described more in detail in [12] and [35], the geometry of the arch is representative of the cross-section of a two-course brick barrel vault with a radial thickness of 0.24 m and an internal radius of 3 m.

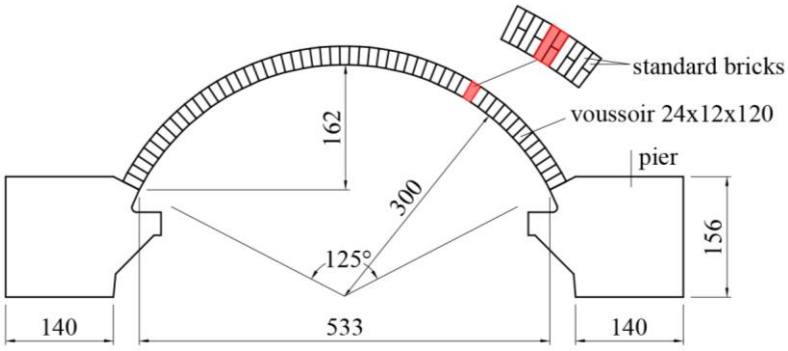

Fig. 1 Geometry of the mockup (in mm).

The arch is composed of 55 voussoirs with a slightly trapezoidal shape compensating for the lack of mortar joints. As shown in Fig. 1, the cross-section of each voussoir represents the scaled dimensions of four adjacent bricks of standard size (60x120x240 mm^3), one positioned with its longest side along the radial plane and two laid on their long narrow side with the short end exposed, as typically observed in Italian two-course brick barrel vaults. This choice was based on practical reasons, as reproducing exactly the real brick pattern would have made the construction of the physical model unduly complicated due to the need to produce and assembly very small voussoirs.

All the blocks (voussoirs and piers) are made of a bicomponent composite material (Plastoform PL, [36]) obtained by mixing a mineral powder with an acrylic polymer in aqueous solution. To form the blocks, the mixture was poured in special silicone moulds (Fig. 2a) created from aluminium matrices shaped as the blocks (Fig. 2b). In the case of the arch voussoirs, the mixture was fluidified by adding a plasticizer (1% of the total weight) to facilitate the pouring.

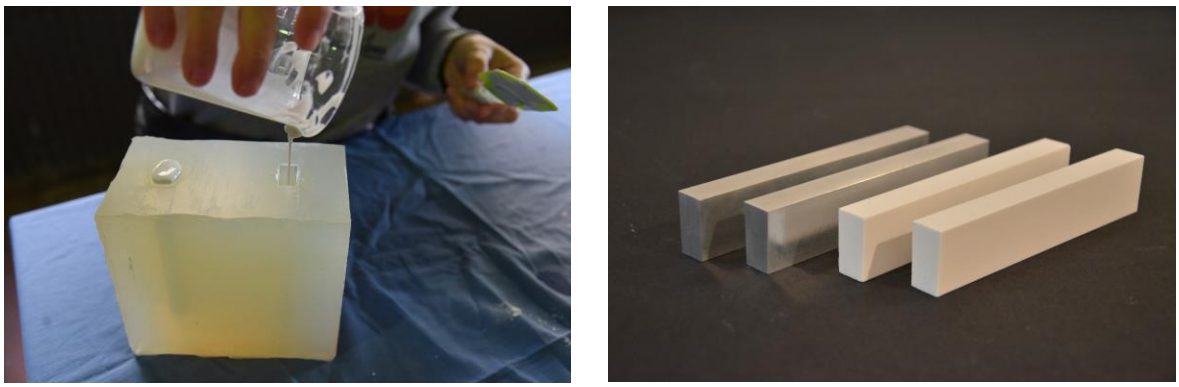

a) b)

Fig. 2 a) Silicone mould used for the production of the arch voussoirs, b) alluminium matrices and bicomponent composite blocks.

An interesting potential of this manufacturing technique is that it allows one to produce very small voussoirs with good dimensional accuracy without requiring any special equipment or large budget. Furthermore, the bicomponent composite blocks have high compressive strength and stiffness with respect to the applied loads (they can be considered rigid and infinitely resistant in compression) as well as high friction (sliding between blocks does not generally occur). These properties, together with the use of no tension dry joints, make the physical model coherent with Heyman's assumptions on the behaviour of masonry structures [28,37]. As such, the arch was expected to behave as a rigid-no tension arch deforming by opening hinges only. The friction angle Φ = 41.2° was measured by testing ten couples of arch voussoirs on an inclined plane. The compressive strength σ_c = 9.1 MPa and the Young's modulus E = 941 MPa were evaluated by testing six prisms with size of about 40x40x80 mm^3 under uniaxial compression. The density ρ of the bicomponent composite material was measured to be 1.64 g/cm^3. The total weight of the mockup (including arch and supporting piers) was about 13.9 kg.

To build the arch, a temporary supporting structure (centering) made of plywood was constructed and positioned directly on the blocks of the piers, which were specially shaped so that no further support

was required (Fig. 3a). The centering was equipped with three regulation screws that allowed it to be adjusted to the required height and removed from underneath when the arch was completely assembled (Fig. 3b-c). Fig. 3d shows a view of the physical model after the removal of the supporting structure.

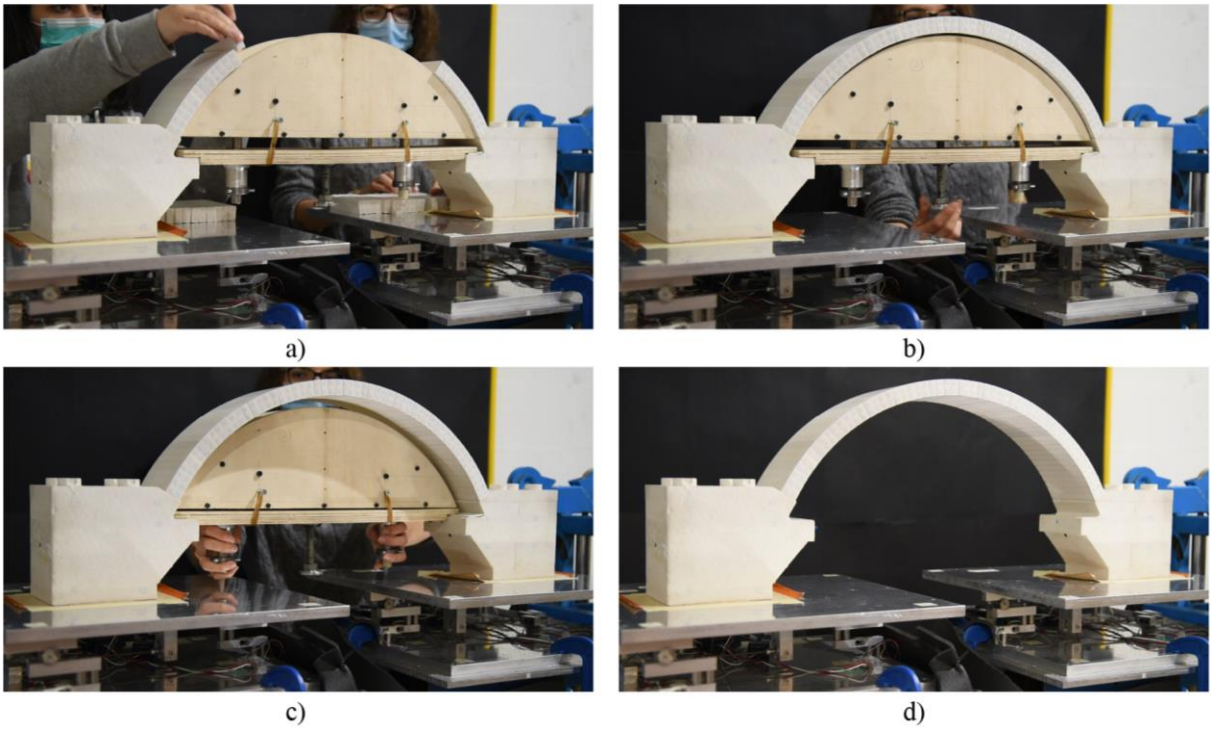

Fig. 3 Construction of the physical model: a) positioning of the arch voussoirs on the plywood centering, b-c) removal of the centering, d) view of the arch after the centering removal.

3. Experimental set-up

To perform the experimental tests, a special testing device was designed, which consists of a steel frame supporting two aluminium squared plates where the two piers of the arch can be placed (Fig. 4). The left support is fixed, whereas the right support can be moved in different directions through a system of guides and stepping motors [38] controlled via software. As shown in Fig. 4a, the stepping motors SM1 and SM2 respectively assign vertical (δ_z) and horizontal (δ_x) displacements and can be activated separately (to impose purely vertical or horizontal displacements) or simultaneously (to produce inclined displacements).

For the purposes of this work, downward vertical, outward horizontal and outward inclined displacements were applied. The direction of the imposed displacement δ was identified with the angle α measured from the vertical (Fig. 4a). As Table 2 shows, thirteen displacement directions were investigated by varying α between 0° and 90°. In the case of α equal to 0° and 90°, which respectively

correspond to purely vertical and horizontal support displacements, the tests were repeated seven times to verify the repeatability of the results.

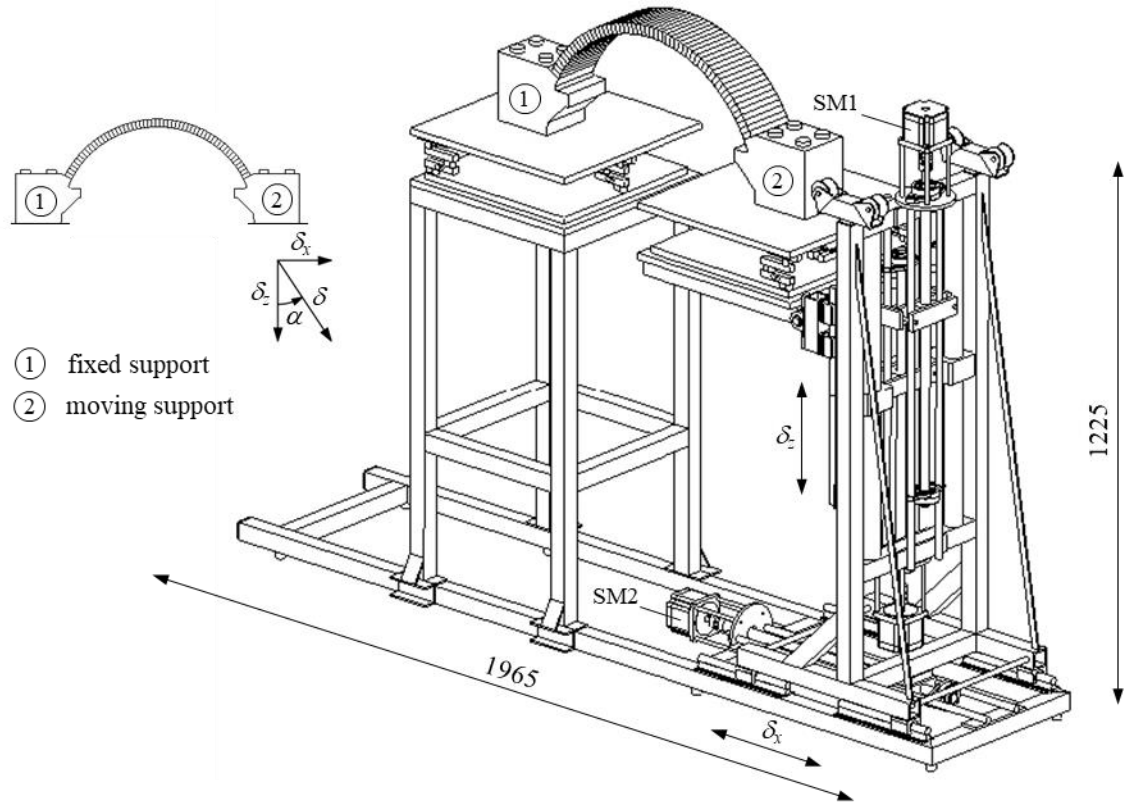

a)

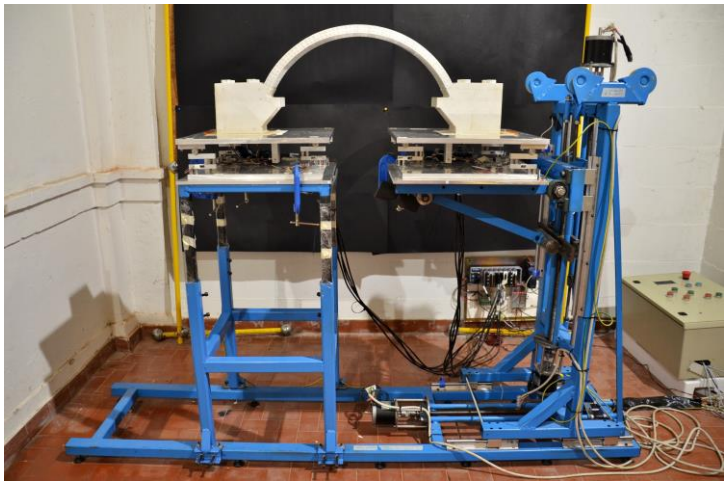

b)

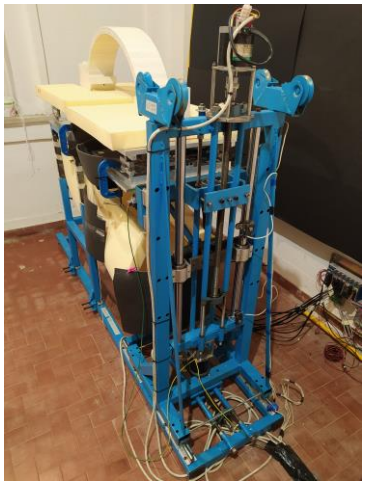

c)

Fig. 4 Testing machine: a) 3D CAD model, b) front view, c) lateral view.

Table 2 Experimental testing programme: number of tests performed for each direction of support displacements investigated (identified with the angle α indicated in Fig. 4a).

α [°]	0	5	10	15	20	25	30	35	40	45	60	75	90
No. of tests	7	1	1	1	1	1	1	1	1	1	1	1	7

The support displacements were applied at very low speeds (maximum 0.04 mm/s) to avoid dynamic effects that would not be compatible with the slow development of phenomena like slow-moving landslides and foundation settlements.

Different measuring systems were implemented to monitor (i) the displacements of the moving support, (ii) the reactions at the base of the mockup and (iii) the displacements of all the individual voussoirs throughout the tests.

The vertical (δ_z) and horizontal (δ_x) components of the imposed displacement δ were tracked by the same software used to impose support displacements.

The reactions at the base of the piers were monitored through a system of load cells, which was built ad hoc and positioned between two squared aluminium plates supported on the testing device (Fig. 5). At each support of the mockup, three load cells (labelled V1, V2 and V3 in Fig. 5c) monitored the vertical component of the reaction, while one load cell (indicated as H1 in Fig. 5c) measured the horizontal component. It is important to highlight that the system of load cells was designed so that the measurement of the horizontal reaction was uncoupled from the measurement of the vertical one. For further details, the reader is referred to [2].

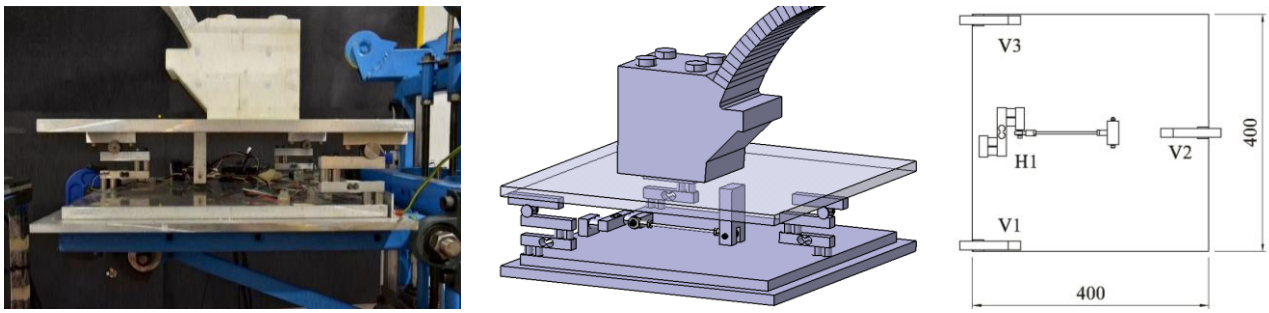

a) b) c)

Fig. 5 System of load cells used to measure the support reactions: a) front view, b) 3D CAD model view, c) 2D view of the lower plate where the load cells are mounted.

The displacements of each block of the mockup were tracked by means of a 2D optical measuring system. The motion was detected through reflective markers, which were placed on the physical model, two per voussoir and five on the piers, for a total of 115 targeted points (Fig. 6). To follow the movements of the markers during the tests, a sequence of images (sampling frequency of 60 Hz) was acquired through a high definition, high-rate digital camera (Dalsa Falcon2 FA-80-4M180-01-R-

4 Megapixels), equipped with an infrared lamp and an infrared filter. The images were then processed by means of an infrared optical acquisition system developed by [39]. A further high-rate digital camera, set at a frame rate of 60 frames per second, was used to record the entire development of the damage mechanism from the undeformed state up to collapse. Both digital cameras were synchronised with the stepping motors and were activated simultaneously with the application of support displacements.

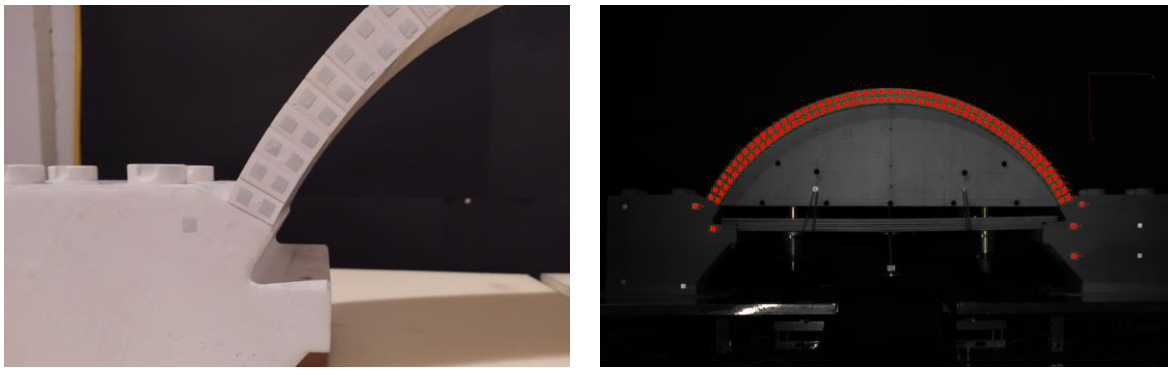

a) b)

Fig. 6 2D optical measuring system used to track the displacements of the blocks: a) reflective markers, b) targeted points.

4. Results

The arch response to large support displacements is described in Section 4.1 in terms of evolution of the arch deformed configuration and collapse mechanisms and in Section 4.2 in terms of support reactions-displacement curves, ultimate displacement capacity, support reactions at collapse, and limit displacement domain (the latter was first introduced by the authors in [35]). The imposed vertical and horizontal displacements are expressed in a dimensionless form as δ_z/L and δ_x/L, where L is the arch span length. Similarly, the vertical and horizontal components of the collapse displacement, hereafter named vertical ($\delta_{z.u}$) and horizontal ($\delta_{x.u}$) collapse displacements, respectively, are normalized by the arch span length L to give $\delta_{z.u}/L$ and $\delta_{z.u}/L$. The vertical and horizontal reactions at the arch springings, hereafter indicated as vertical (R_z) and horizontal (R_x) support reactions, are expressed as dimensionless variables as R_z/W and R_x/W, where W is the arch weight. The vertical reactions at the arch supports are obtained by subtracting the weight of the piers from the total vertical reactions measured by the load-cells at the base of the mockup.

4.1. Evolution of the arch deformed configuration and collapse mechanisms

A first insight in the evolution of the arch deformed configuration with the increase of support displacements was gained by examining the recordings of the experimental tests taken by the high-rate camera (Section 4.1.1). The arch performance was then further investigated by performing graphic statics and analysing the evolution of the voussoirs' displacements during the tests (Section 4.1.2).

4.1.1. Preliminary observations

The first aim was to identify the failure modes obtained when varying the direction of the imposed displacement (angle α). For this purpose, Table 3 reports the hinge position at collapse. The joints where hinges are located at the intrados (I) or extrados (E) are numbered from left to right, being joints no. 1 and 56 the ones corresponding to the left and right supports, respectively (see Fig. 7). For $\alpha = 0°$ and $\alpha = 90°$, the hinge location is presented for one representative test only, as the test results were found to be highly repeatable (see Section 4.3). In all the experiments, the three hinges identified as A, B and C (from the left fixed support) were always the first to appear, while hinge D opened at collapse. In the case of $\alpha = 90°$, a fifth hinge, E, also appeared at collapse in most of the tests due to the symmetry in geometry and displacement loading.

Table 3 Hinge position at collapse (I = intrados, E = extrados; the numeration of the joints where hinges occurred is shown in Fig. 7).

α [°]	Joint no.				
	hinge A	hinge B	hinge C	hinge D	hinge E
0(*)	9-I	28-E	56-E	1-E	-
5	9-I	31-E	56-E	1-E	-
10	9-I	31-E	56-E	1-E	-
15	10-I	31-E	not visible	1-E	-
20	9-I	30-E	not visible	1-E	-
25	9-I	28-E	not visible	1-E	-
30	9-I	28-E	not visible	1-E	-
35	10-I	28-E	45-I	1-E	-
40	10-I	28-E	44-45-46-I	1-E	-
45	11-I	28-E	44-45-46-I	1-E	-
60	11-I	28-E	44-I	1-E	-
75	11-I	28-E	45-I	1-E	-
90(**)	12-I	28-E	45-I	1-E	56-E

(*) Results obtained in test #7 (see Section 4.3)

(**) Results obtained in test #3 (see Section 4.3)

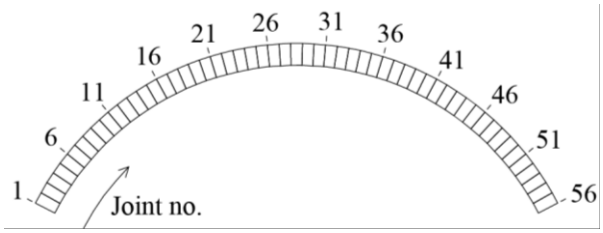

Fig. 7 Numeration of the joints where hinges occurred at collapse.

As Table 3 shows, for every α, hinges A and B appeared at a very similar location at the intrados and extrados, respectively, and hinge D always opened at the fixed support at the extrados. In contrast, hinge C was located at the right support at the extrados for $\alpha = 0°\div10°$, at the right haunch at the intrados for $\alpha = 35°\div90°$, and it was not visible for $\alpha = 15°\div30°$. On the basis of the position of hinge C and the number of hinges occurring at collapse, four final hinge configurations were identified when varying α. For each of them, the arch response from the opening of the initial hinges to collapse is described in detail in the following paragraphs.

Response in the range $\alpha = 0°\div10°$

Fig. 8 and Fig. 9 present the evolution of the arch deformed configuration for $\alpha = 0°$ (test #7) and $\alpha = 10°$, respectively. Looking at the early stages of the tests (Fig. 8a and Fig. 9a), it can be seen that hinges A, B and C were not initially visible and appeared, generally not all at once, only as the right support moved further (Fig. 8b-c and Fig. 9b-c-d). As shown more clearly in Fig. 10, hinges A and B were initially distributed among consecutive joints and concentrated in single joints only with the increase of support displacements. Further insight in this behaviour, which was found to occur for every value of α, will be provided in Section 4.1.2.

As already observed in the literature for arches subjected to purely vertical displacements (see [4-7,12,14]), in the range $\alpha = 0°\div10°$, hinge A appeared at the intrados and the two consecutive hinges B and C occurred at the extrados (Fig. 8c and Fig. 9d). The hinge location followed the sequence I-E-E (E = extrados; I = intrados) from the left fixed support: hinge A was located at the left haunch; hinge B appeared close to mid-span; hinge C occurred at the right support. It is interesting to note that hinge C decreased in width with increasing α, until becoming barely visible for $\alpha = 10°$ (compare Fig. 8e and

Fig. 9e). All the three hinges generally remained in their initial position and did not move with the increase of support displacements.

As Fig. 8e and Fig. 9e show, collapse occurred by an asymmetrical four-hinge mechanism when a fourth hinge, D, appeared at the left support at the extrados. As soon as the collapse mechanism was activated, the part of the arch between hinge D and hinge A started to rotate upwards around hinge D. Simultaneously, the part of the arch between hinges B and C, which rotated upwards up to the opening of hinge D, started to rotate downwards around hinge C, which gradually closed (see Fig. 8f and Fig. 9f).

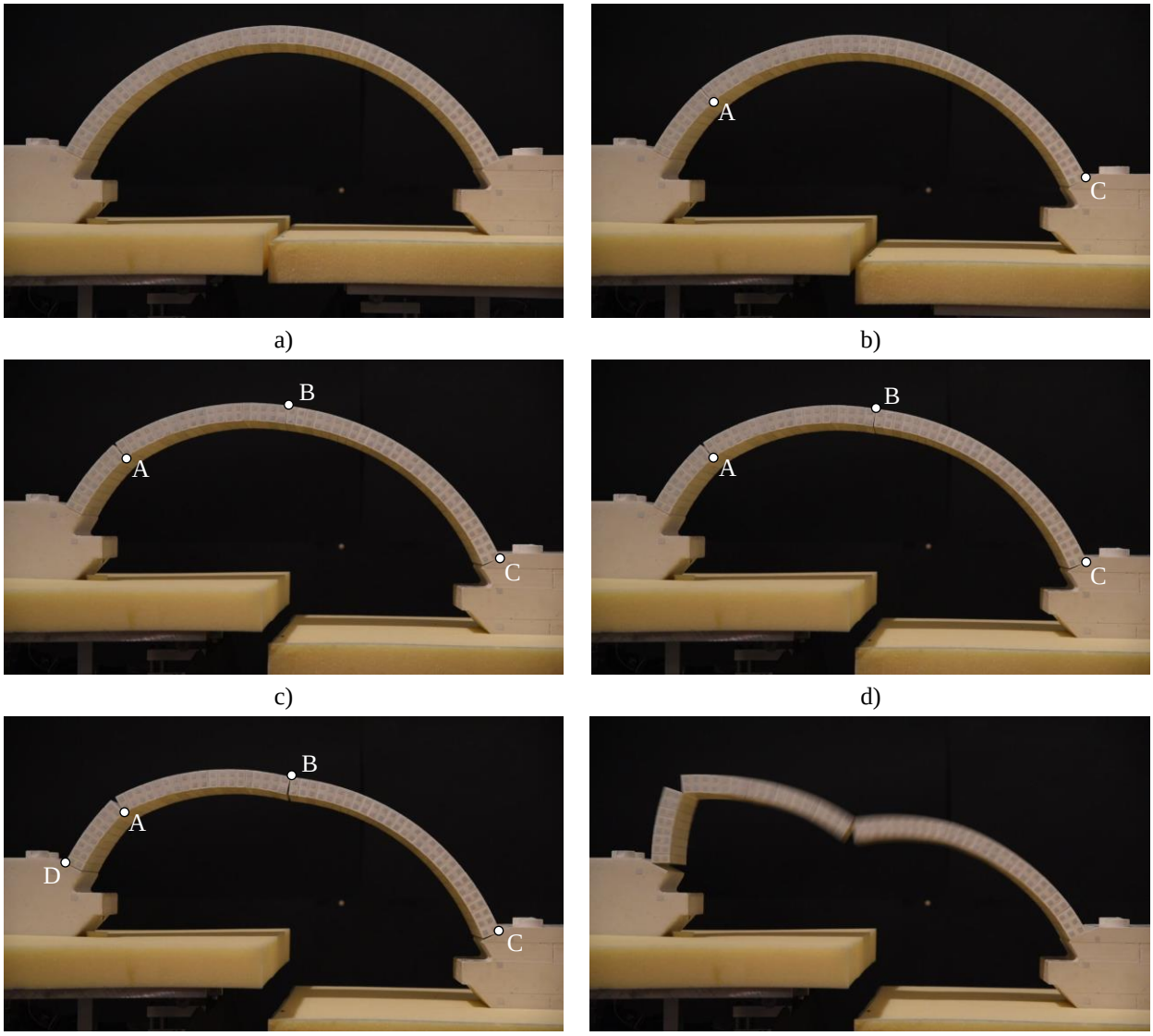

a) b) c) d) e) f)

Fig. 8 Damage evolution for $\alpha = 0°$: a) δ_z/L = 1.9%, b) δ_z/L = 6.6%, c) δ_z/L = 12.2%, d) δ_z/L = 13.1%, e) collapse for $\delta_{z,u}/L$ = 16.5%, f) unstable configuration corresponding to δ_z/L = 16.5%.

Fig. 8f and Fig. 9f show an unstable configuration reached by the arch just before the full failure. It can be seen that hinge C fully closed and a new hinge appeared at the intrados between hinge B and the right support. However, this hinge did not contribute to the activation of the collapse mechanism because it opened when the arch was already in motion. In this regard, it is worth noting that the final hinge configuration obtained at collapse for α between 0° and 10° (sequence E-I-E-E) is kinematic admissible because hinge C can close, allowing block B-C to rotate downwards. In the existing literature, this behaviour was observed only by the authors in [12].

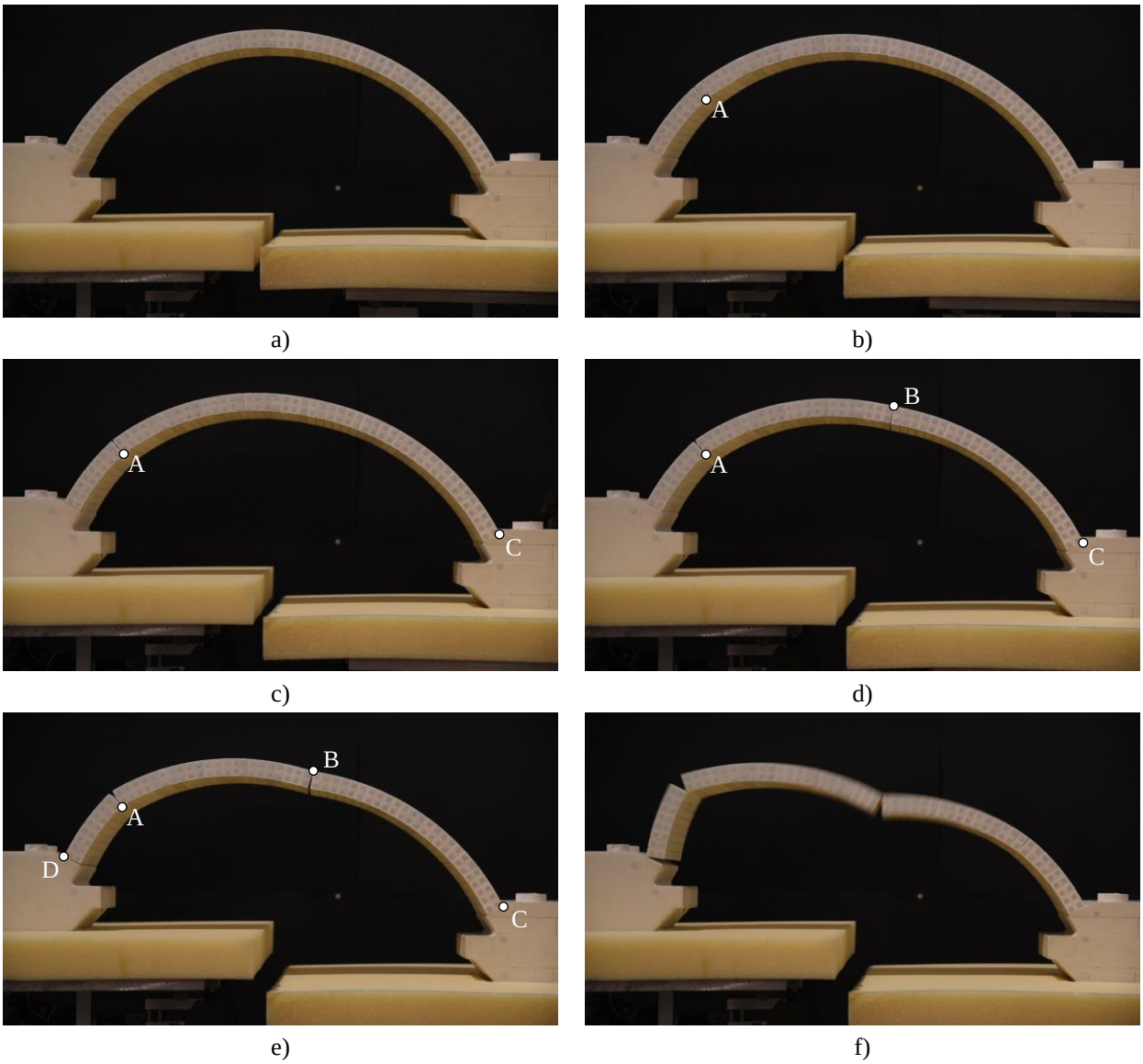

a) b) c) d) e) f)

Fig. 9 Damage evolution for α = 10°: a) δ_z/L = 3.8%, b) δ_z/L = 5.6%, c) δ_z/L = 7.5%, d) δ_z/L = 9.4%, e) collapse for $\delta_{z,u}/L$ = 11.9%, f) unstable configuration corresponding to δ_z/L = 11.9%.

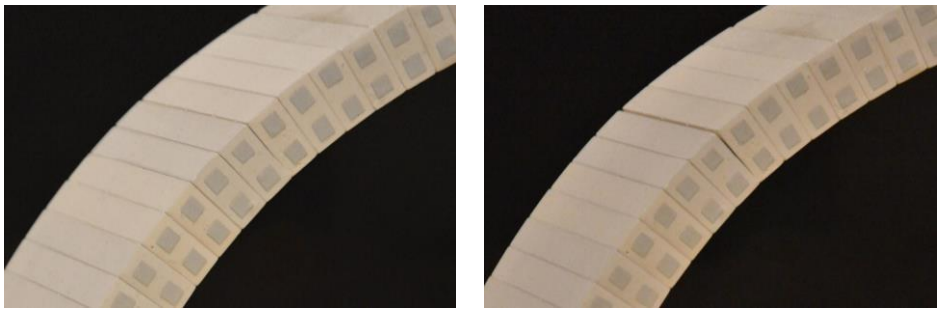

a) b)

Fig. 10 Evolution of the hinge opening with the increase of support displacements: a) hinge distributed over consecutive joints, b) hinge concentrated in one single joint.

Response in the range 15°÷30°

Fig. 11 presents the evolution of arch deformed configuration with the increase of support displacements for α = 25°. In the range α = 15°÷30°, only two hinges, A and B, were visible prior to collapse (Fig. 11a-b-c-d). The intrados hinge A opened at the same position at the left haunch (joint no. 9) no matter α, whereas the extrados hinge B was located next to mid-span and appeared closer to the keystone as α increased. Hinges A and B did not generally change position as the right support moved, apart from two exceptions. For α =15°, hinge A moved upwards by one voussoir just before collapse. For α = 25°, hinge B moved by four voussoirs towards the crown for a vertical displacement equal to about 50% of the collapse displacement (see Fig. 11b).

As shown in Fig. 11e for α = 25°, in the range α = 15°÷30°, the arch collapsed when hinge D appeared at the left support at the extrados, causing block D-A to rotate upwards. The presence of only three hinges at the final collapse state, however, prevented the identification of a clear failure mode. According to the experimental studies on arches on moving supports (see Section 1), at least four hinges are needed for collapse to occur unless the arch has a very large thickness-to-radius ratio and a small angle of embrace (which is not the case of the arch under consideration). In this respect, it is worth noting that the hinge visible at the intrados between hinge B and the right support in Fig. 11f, which shows an unstable configuration occurring just before the full failure, was not involved in the activation of the collapse mechanism because it appeared when the arch was already in motion. In view of these considerations, further investigation on hinge opening will be presented in Section 4.1.2

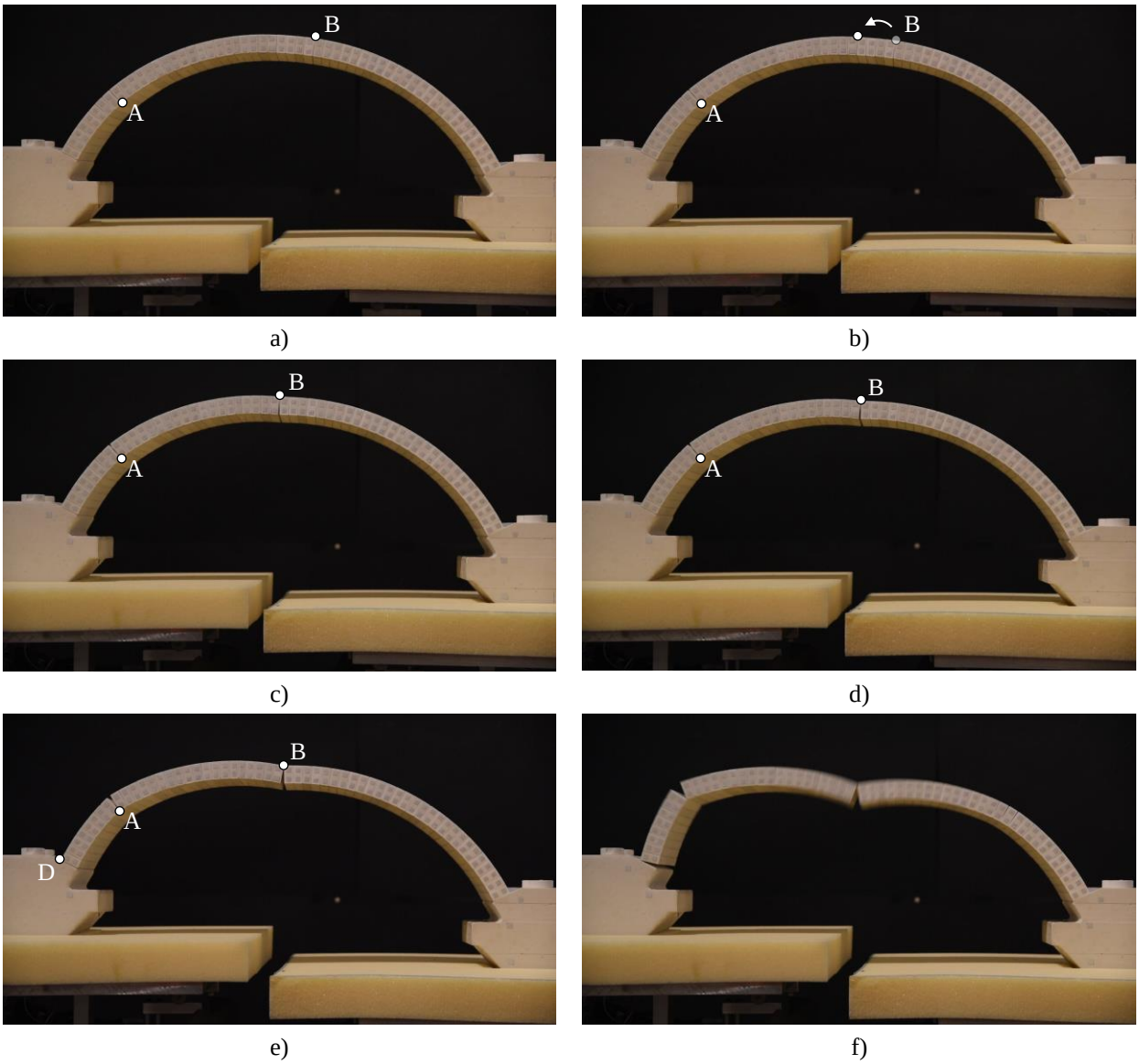

Fig. 11 Damage evolution for $\alpha = 25°$: a) $\delta_z/L = 2.8\%$, b) hinge movement for $\delta_z/L = 3.8\%$, c) $\delta_z/L = 4.7\%$, d) $\delta_z/L = 5.6\%$, e) collapse for $\delta_{z,u}/L = 7.6\%$, f) unstable configuration corresponding to $\delta_z/L = 7.6\%$.

Response in the range $\alpha = 35°\div75°$

Fig. 12 and Fig. 13 depict the evolution of arch deformed configuration throughout the tests for $\alpha = 35°$ and $\alpha = 75°$, respectively. In the range $\alpha = 35°\div75$, the three initial hinges A, B and C alternated between the intrados and extrados according to the sequence I-E-I (Fig. 12d and Fig. 13b). Regardless of the value of α, hinges A and B initially appeared at the left haunch at joint no. 9 and at the left side of the keystone, respectively (Fig. 12a-b and Fig. 13a). Differently from what was observed in the range $\alpha = 0°\div10°$, hinge C did not appear at the right support at the extrados but at the right haunch at the intrados.

The initial location of hinge C was more difficult to assess, as the hinge was distributed over consecutive joints from its opening up to collapse for most of the values of α under study (see Table 3).

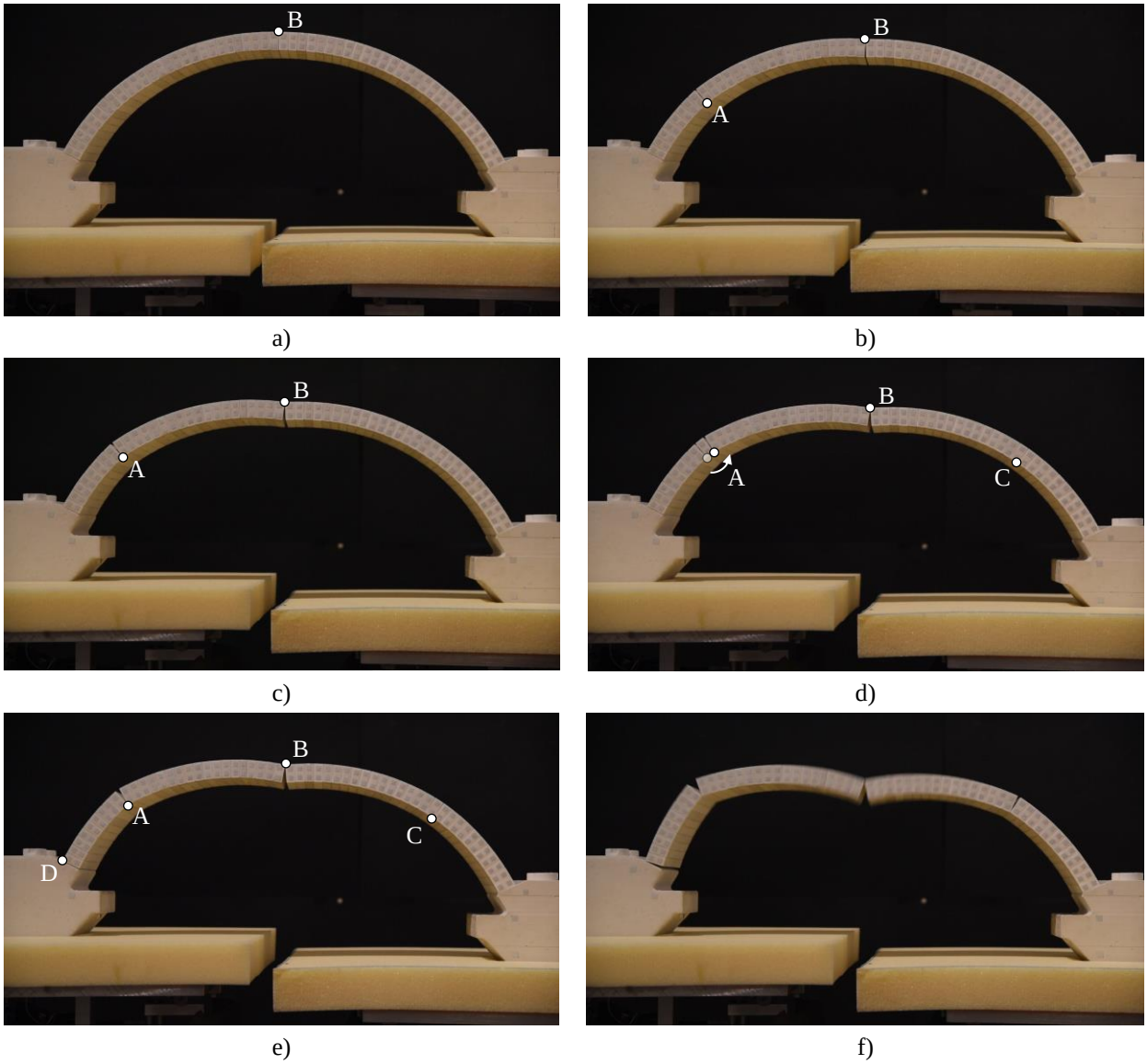

Fig. 12 Damage evolution for α = 35°: a) δ_z/L = 1.9%, b) δ_z/L = 3.2%, c) δ_z/L = 4.7%, d) hinge movement for δ_z/L = 5.5%, e) collapse for $\delta_{z,u}/L$ = 5.5%, f) unstable configuration corresponding to δ_z/L = 5.5%.

As support displacements increased, the extrados hinge B did not change position, while the intrados hinges A and C moved towards the crown (Fig. 12d and Fig. 13c). In particular, hinge A moved upwards by one voussoir for α equal to 35° and 40° (see Fig. 12d for α = 35°) and by two voussoirs for α between 45° and 75° (compare Fig. 13a and Fig. 13e for α = 75°). In the case of α equal to 35°, 45° and 60°, a change in the position of hinge A took place just before collapse (see Fig. 12d for α = 35°). The

movement of hinge A generally produced a sudden change in the arch geometry, while that of hinge C was generally more gradual and not always easy to detect.

Similarly to what occurred for $\alpha = 0° \div 10°$, also for $\alpha = 35° \div 75°$ collapse was triggered by the opening of a fourth hinge, D, at the left support at the extrados (Fig. 12e and Fig. 13e). Fig. 12f and Fig. 13f show the progress of the collapse mechanism towards the full failure. Although changes in the location of hinge C were occasionally observed, the final hinge position reported in Table 3 is the one obtained when hinge D appeared and the collapse mechanism was activated. In this respect, it should be noted that the final position at collapse of the intrados hinges A and C became more symmetrical with respect to the vertical axis of the arch as α increased (compare Fig. 12e and Fig. 13e).

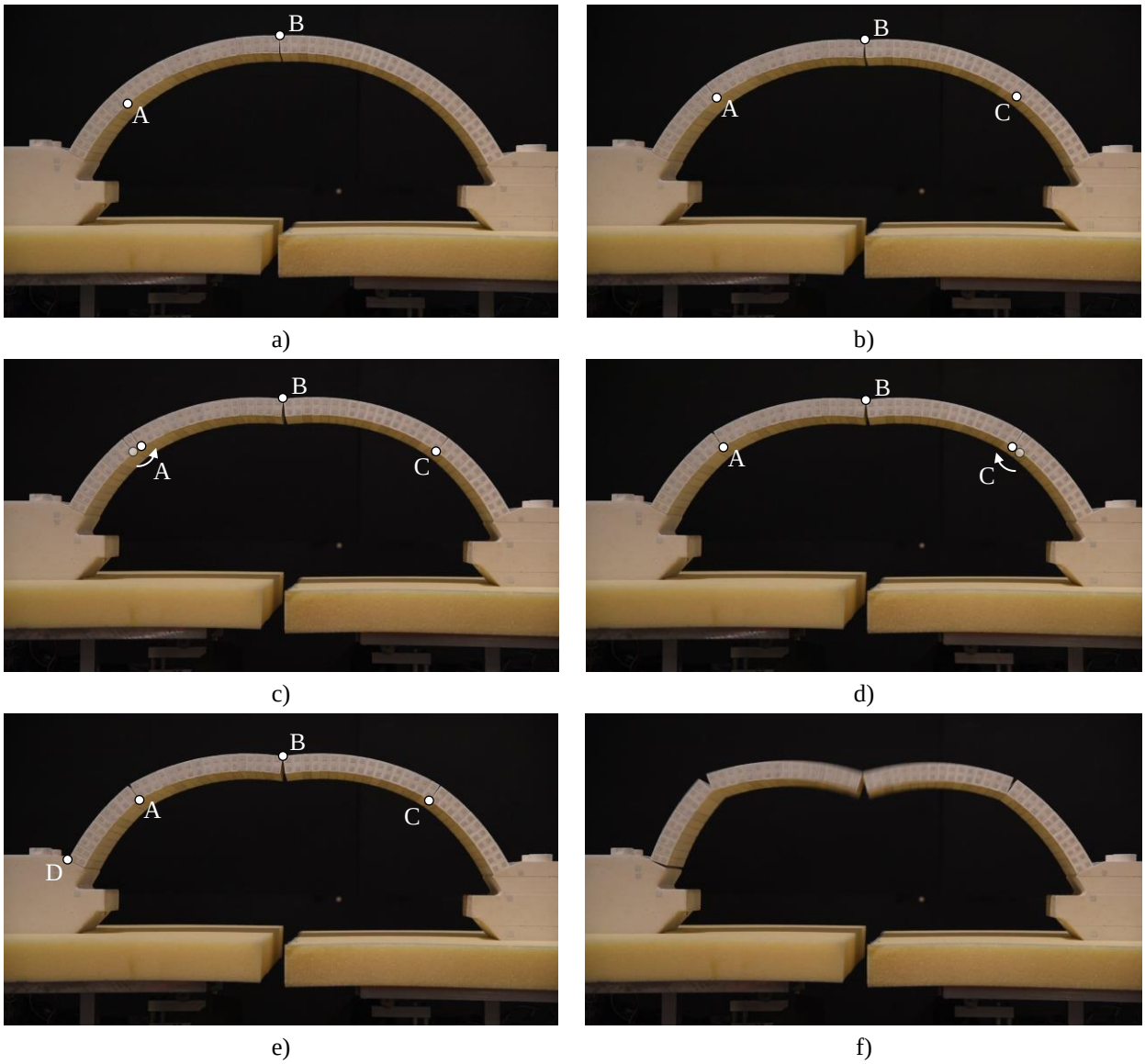

Fig. 13 Damage evolution for $\alpha = 75°$: a) $\delta_z/L = 0.6\%$, b) $\delta_z/L = 0.8\%$, c-d) hinge movement for $\delta_z/L = 1.0\%$, e) collapse for $\delta_z/L = 1.0\%$, f) unstable configuration corresponding to $\delta_z/L = 1.0\%$.

Response for $\alpha = 90°$

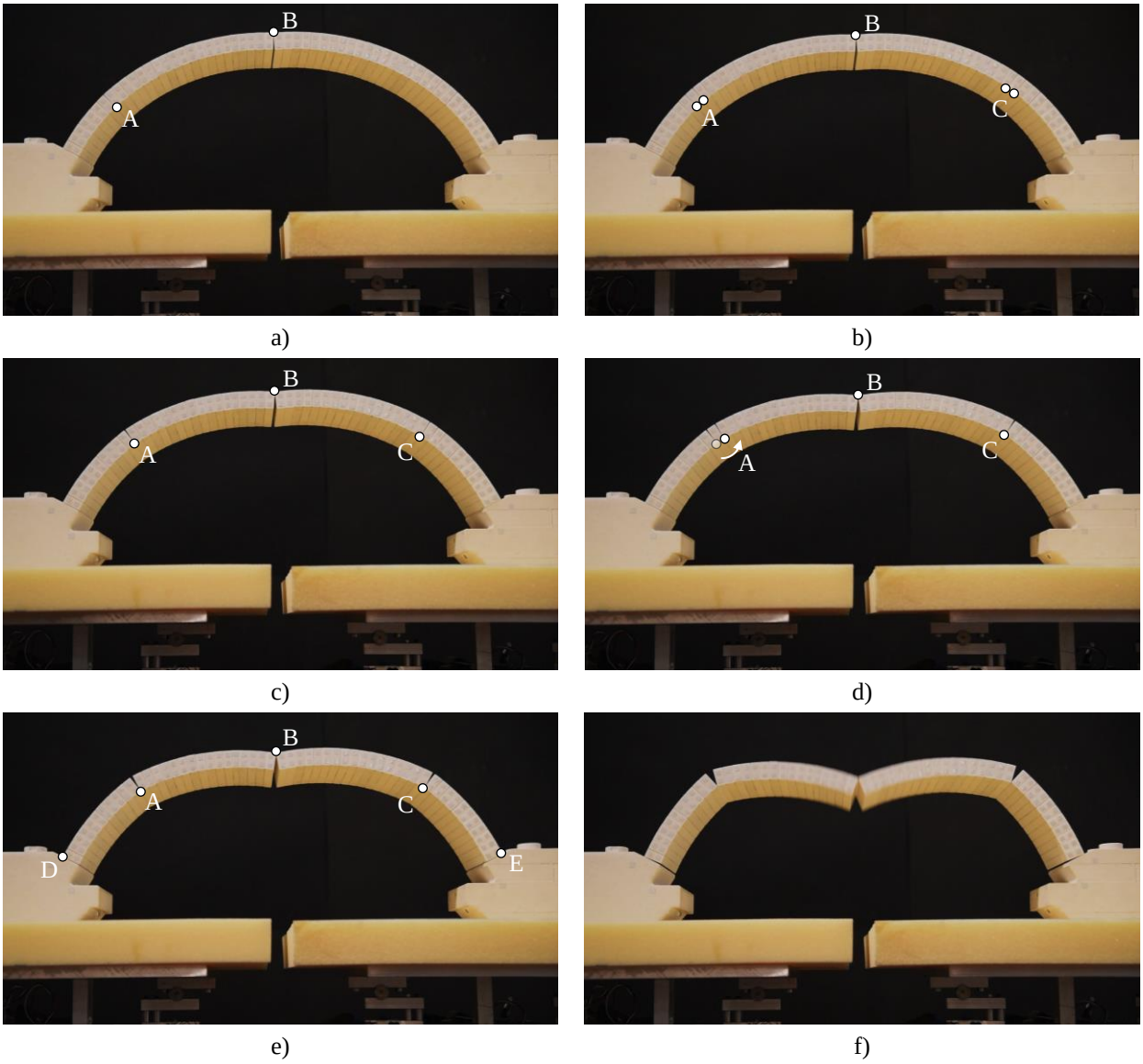

Fig. 14 Damage evolution for $\alpha = 90°$: a) $\delta_x/L = 2.8\%$, b) $\delta_x/L = 3.2\%$, c) $\delta_x/L = 3.4\%$, d) hinge movement for $\delta_x/L = 3.7\%$, e) collapse for $\delta_{x,u}/L = 3.7\%$, f) unstable configuration corresponding to $\delta_x/L = 3.7\%$.

In the case of $\alpha = 90°$, the arch response prior to collapse was the same as that observed in the range $\alpha = 35°\div75°$: hinges A, B and C were located in the sequence I-E-I and, in addition, the intrados hinges A and C moved towards the crown with the increase of support displacements (Fig. 14a-b-c-d). However, while a four-hinge collapse mechanism was observed for α up to 75°, a five-hinge collapse mechanism generally occurred for $\alpha = 90°$ (see Fig. 14e for test#3). In this latter case, as soon as hinges D and E opened at the supports at the extrados, the parts of the arch between the supports and the intrados hinges A and C started to rotate upwards and the crown descended (Fig. 14f). Although the keystone

prevented the opening of a hinge exactly at mid-span, the collapse mechanism was almost symmetrical, as hinges appeared at both supports and, furthermore, the intrados hinges A and C were located in a symmetrical position with respect to the vertical axis of symmetry of the arch. This response well approximates that expected for a perfectly symmetrical arch, which would collapse by a symmetrical five-hinge mechanism. However, in some of the tests repeated for α = 90°, an asymmetrical collapse mechanism, clearly due to the slight imperfections and not perfect symmetry of the physical model, was also observed to occur (see Section 4.3).

4.1.2. Further insight in the arch response in the range α = 15°÷30°

In an attempt to better understand the collapse mechanism in the range α = 15°÷30°, the arch deformed configuration at collapse (i.e. as soon as hinge D has started to open) was analysed through graphic statics [40,41] by computing the thrust line passing through the three hinges A, B and D (Fig. 15b-c-d-e). Graphic statics can help in detecting the opening of further hinges because the thrust line at collapse is unique and passes through as many hinges as needed to develop a mechanism [37,42]. The results from graphic statics for α = 0° and α = 35° are provided for comparison in Fig. 15a and Fig. 15f, respectively. In these cases, as expected, the thrust line drawn considering the location at collapse of the three initial hinges A, B and C also passes through hinge D, which triggered the collapse mechanism.

For α = 15° (Fig. 15b), the thrust line touches the external boundary of the arch at the extrados at the right support, indicating that a fourth hinge (C) occurred there and, thus, the final hinge configuration at collapse followed the sequence E-I-E-E, as obtained for α = 0°÷10°. In contrast, for α = 20°÷30°, a fourth hinge cannot be identified because the thrust line is not tangent to the boundary of the arch in any further section. However, it is interesting to see that the thrust line is close to touch the intrados at the right haunch, being almost tangent to the internal boundary in correspondence to some consecutive joints, and it moves closer to the intrados as α increases (see Fig. 15c-d-e).

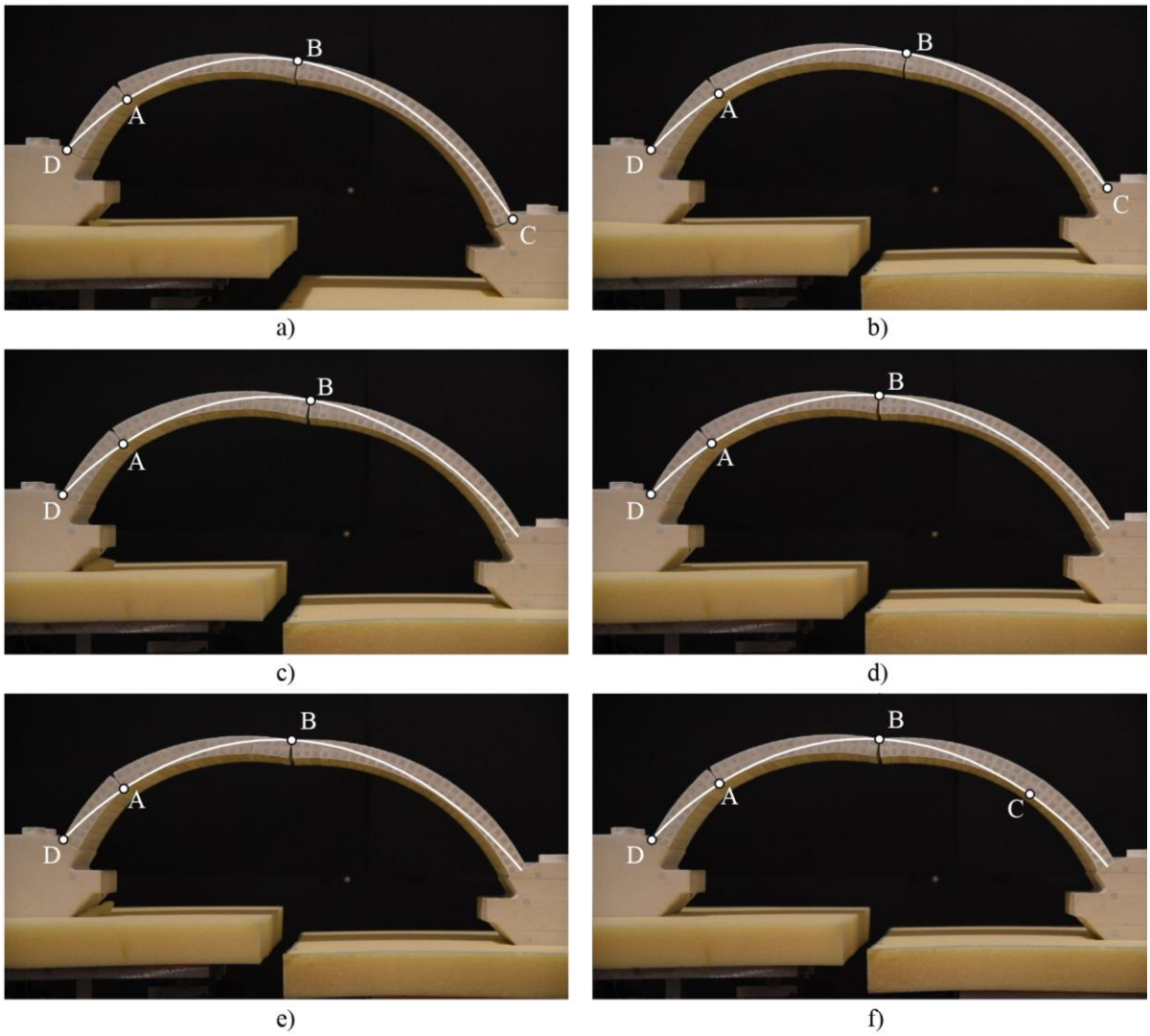

Fig. 15 Thrust line obtained by graphic statics: a) $\alpha = 0°$, b) $\alpha = 15°$, c) $\alpha = 20°$, d) $\alpha = 25°$, e) $\alpha = 30°$, f) $\alpha = 35°$.

To gain further insight into the arch response in the range $\alpha = 20°\div30°$, the displacements of the arch voussoirs as measured during the tests by the infrared camera were analysed. In particular, for the voussoirs coloured in grey in Fig. 16a, the evolution throughout the test of the vertical displacement was investigated (note that, for each voussoir, the vertical displacement of the centroid of the marker located at intrados was considered). In view of the hinge configurations identified for the other values of α, the aim was to understand whether, in the range $\alpha = 20°\div30°$, the right part of the arch between hinge B and the right support behaved as a single block, potentially rotating around a further hinge at the springings, or experienced any relative rotations between different parts with the increase of support displacements. This study was carried out for every α between 0° and 90° to compare the response in the range $\alpha = 20°\div30°$ with that in the other ranges.

For some representative values of α, Fig. 17 plots the vertical displacements of the voussoirs under study minus the imposed vertical displacement δ_z (quantity hereafter labelled $\Delta_{z,v}$) as a function of the imposed normalized vertical displacement δ_z/L. The vertical displacement measured for the right pier (indicated as RS) is also plotted for reference. Note that positive and negative values of $\Delta_{z,v}$ simply indicate that the vertical displacements of the voussoirs are larger or smaller than the imposed displacement δ_z, respectively.

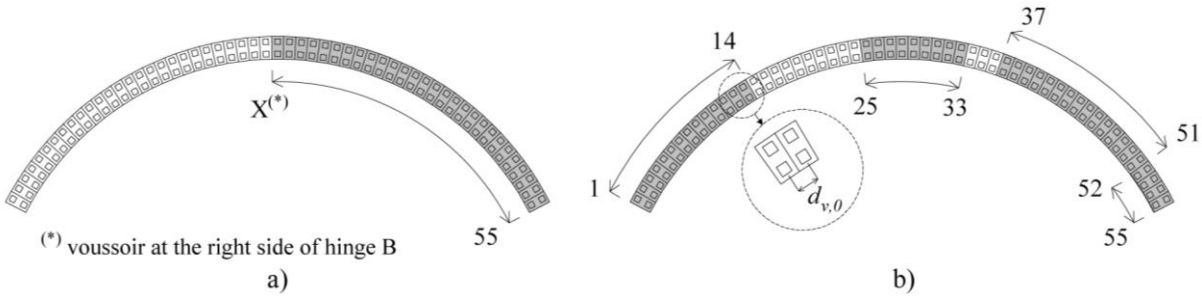

Fig. 16 Voussoirs taken into consideration to analyse: a) the evolution of the vertical displacements of the voussoirs, b) the change in the distance between adjacent voussoirs (Δd_v) with respect to the initial distance $d_{v,0.}$

For α between 0° and 15° (Fig. 17a-b-c), $\Delta_{z,v}$ generally increases in absolute value with the increase of support displacements. At each displacement increment, the vertical displacements of the voussoirs are smaller than the imposed displacement and increase with their distance from the right support. This trend indicates that the entire set of voussoirs under study rotated upwards around hinge C up to collapse. For α equal to 15° only (Fig. 17c), a slight decrease in $\Delta_{z,v}$, corresponding to a slight downward rotation, is observed for the voussoirs closer to hinge B (no. 31÷37) from a vertical displacement equal to about 7% of the arch span length L. Comparing the maximum values of $\Delta_{z,v}$ obtained prior to collapse, it can also be seen that the upward rotation of the set of voussoirs considered decreases with increasing α. Such a decrease reflects the decrease in the width of hinge C observed in the tests as α increases from 0° to 10°.

For α = 20° (Figure 18d), the whole set of voussoirs under study experiences a slight rotation upwards up to δ_z/L = 4.1%. Beyond this value, it rotates downwards until the initial rotation is fully recovered ($\Delta_{z,v}$ is almost zero for all the markers) for δ_z/L equal to about 7.9 %. This behaviour clearly indicates that a hinge (C) gradually opened and then closed at the right support at the extrados. When the imposed

displacements increase further, the upper voussoirs of the set (between no. 30 and 44) start to rotate downwards. This downward rotation, which increases with increasing support displacements until collapse is reached, suggests that hinge C opened at the right haunch at the intrados after closing at the right support at the extrados. However, this hinge is likely to appear in the form of minor and distributed openings rather than a fully developed hinge, since, at collapse, the thrust line did not touch the arch intrados at the right haunch, but it was almost tangent to it in correspondence to several consecutive joints (see Fig. 15c).

For α between 25° and 75° (see Fig. 17e-f-g-h for α equal to 25°, 30°, 35° and 75°, respectively), the voussoirs between no. 28 and no. 45 experience a downward rotation, increasing with increasing α, from the application of support displacements up to collapse. Since no hinge was detected at the right haunch for α equal to 25° and 30°, it is likely that, for these values of α, minor and distributed openings occurred there, as already observed for α = 20°.

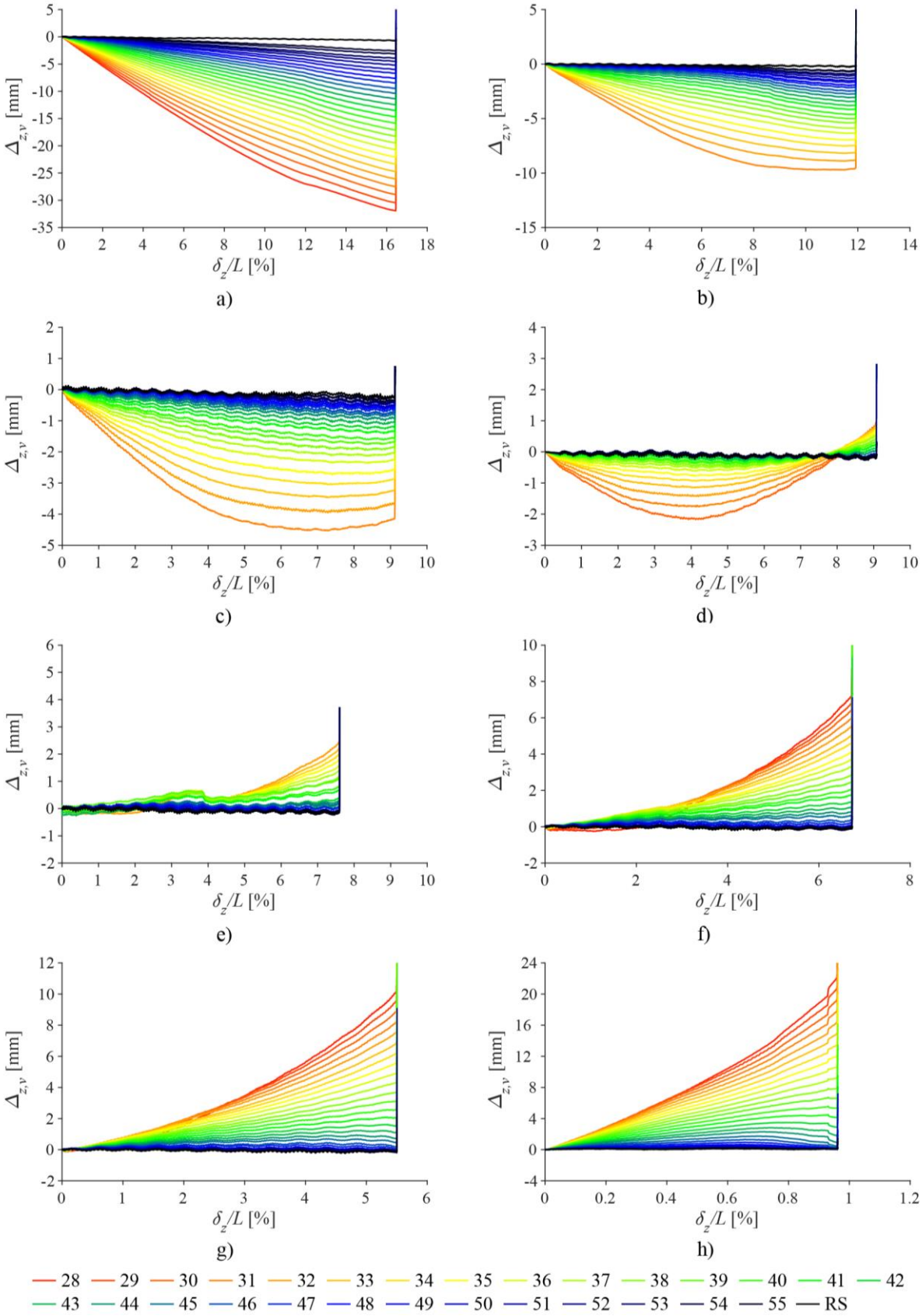

Fig. 17 Vertical displacement of the voussoirs coloured in grey in Fig. 16a minus the imposed vertical displacement, $\Delta_{z,v}$, vs. imposed normalized vertical displacement, δ_z/L: a) α = 0°, b) α = 10°, c) α = 15°, d) α = 20°, e) α = 25°, f) α = 30°, g) α = 35°, h) α = 75°.

Further insight into the occurrence of minor and distributed openings was gained by analysing the evolution of the distance between consecutive voussoirs in the sections of the arch where hinges were expected to appear. This study was carried out for hinge C, which was found to likely occur in the form of minor and distributed openings in the range $\alpha = 20° \div 30°$, as well as for hinges A and B, which were observed to be slightly distributed over consecutive joints in the early stages of the tests for every value of α (see Section 4.1.1).

For four representative angles α ($\alpha = 0°$, $\alpha = 20°$, $\alpha = 30°$, and $\alpha = 75°$), Fig. 18 plots the change in the distance between the markers of adjacent voussoirs, denoted as Δd_v, as a function of the normalized vertical displacement δ_z/L. In Fig. 19, an enlarged view of the y-axis of Fig. 18b-c is presented. For each value of δ_z, Δd_v is defined as the difference between the distance d_v obtained for the imposed displacement and its initial value $d_{v,o}$ (indicated in Fig. 16b). The voussoirs under study are coloured in grey in Fig. 16b. Voussoirs no. 1÷14 (markers at the extrados) and no. 25÷33 (markers at the intrados) were considered to detect the opening of hinges A and B. Two sets of voussoirs were analysed in the case of hinge C due to the different locations at which this hinge appeared depending on α. In particular, attention was paid to voussoirs no. 37÷51 (markers at the extrados) and no. 52-55 (markers at the intrados) for α between 20° and 75° and α between 0° and 10°, respectively. In the case of this latter range of α, since hinge C opened at the right support, the distance between the intrados marker of voussoir no. 55 and one marker placed on the right pier (labelled as RS) was also analysed.

Regardless of α, for all the three hinges A, B and C (except for hinge C in the range $\alpha = 20° \div 30°$), as support displacements increase, the distance between consecutive voussoirs increases, first slightly for several pairs of voussoirs and then more significantly for one pair of voussoirs only (see Fig. 18a-d as well as Fig. 18b-c and Fig. 19a-b on the left and in the middle). This result proves that, when the imposed displacements are small, the arch accommodates the changes in the geometry by forming minor and distributed openings. In contrast, when support displacements increase and the changes in the geometry become more important, the distributed openings concentrate in single joints where hinges fully open. It is worth noting that this behaviour differs from that of a rigid-no tension arch, in which three hinges would appear as soon as one or both supports move [28].

As already mentioned above, a different response is obtained for hinge C in the range $\alpha = 20° \div 30°$. As shown in Fig. 18b-c and Fig. 19a-b on the right, the distance between consecutive voussoirs slightly increases for several pairs of voussoirs up to collapse. This result not only confirms the presence of minor and distributed openings at the right haunch at the intrados for α between 20° and 30°, but also shows that an increase in the distance not larger than few tenth of a millimetre for each pair of consecutive voussoirs is sufficient to allow the part of the arch between hinge B and the right haunch to rotate downwards (see Fig. 17d-e-f). It is worth noting that, as α increases from 20° to 90°, the distance between voussoirs at the right haunch increases more significantly for one or a few pairs of consecutive voussoirs (see Fig. 18b-c-d on the right). This indicates that the minor and distributed openings are gradually replaced by fully developed hinges. This result was expected because a hinge was clearly visible at the intrados at the right haunch for every α between 35° and 90°.

Looking at Fig. 18, a further interesting remark on hinge opening can be put forward. Comparing the position at which hinges A, B and C occur when varying α, it can be seen that, for $\alpha = 0°$ (Fig. 18a), hinges A and C appear and fully develop for smaller imposed vertical displacements δ_z with respect to hinge B, which significantly opens only for values of δ_z/L larger than about 12%. In contrast, as α increases, hinges A and B fully open for more similar values of imposed displacement. The full opening of the intrados hinge C, however, is more difficult to detect, since the increase in the distance between voussoirs at the right haunch is generally small and can involve more than one joint.

It is worth noting that the hinge movement can be easily identified in Fig. 18 through the decrease and increase in the distance between markers in correspondence of two consecutive joints (Fig. 18a-c). As shown in Fig. 18a (on the left), the movement of hinge A towards the crown, occurring for every α equal or larger than 35°, is usually very abrupt. Conversely, the change in the position of hinge C, which takes place for every α larger than 40°, is generally more gradual. Note that the hinge movement was not always captured by the infrared camera when it occurred just before collapse.

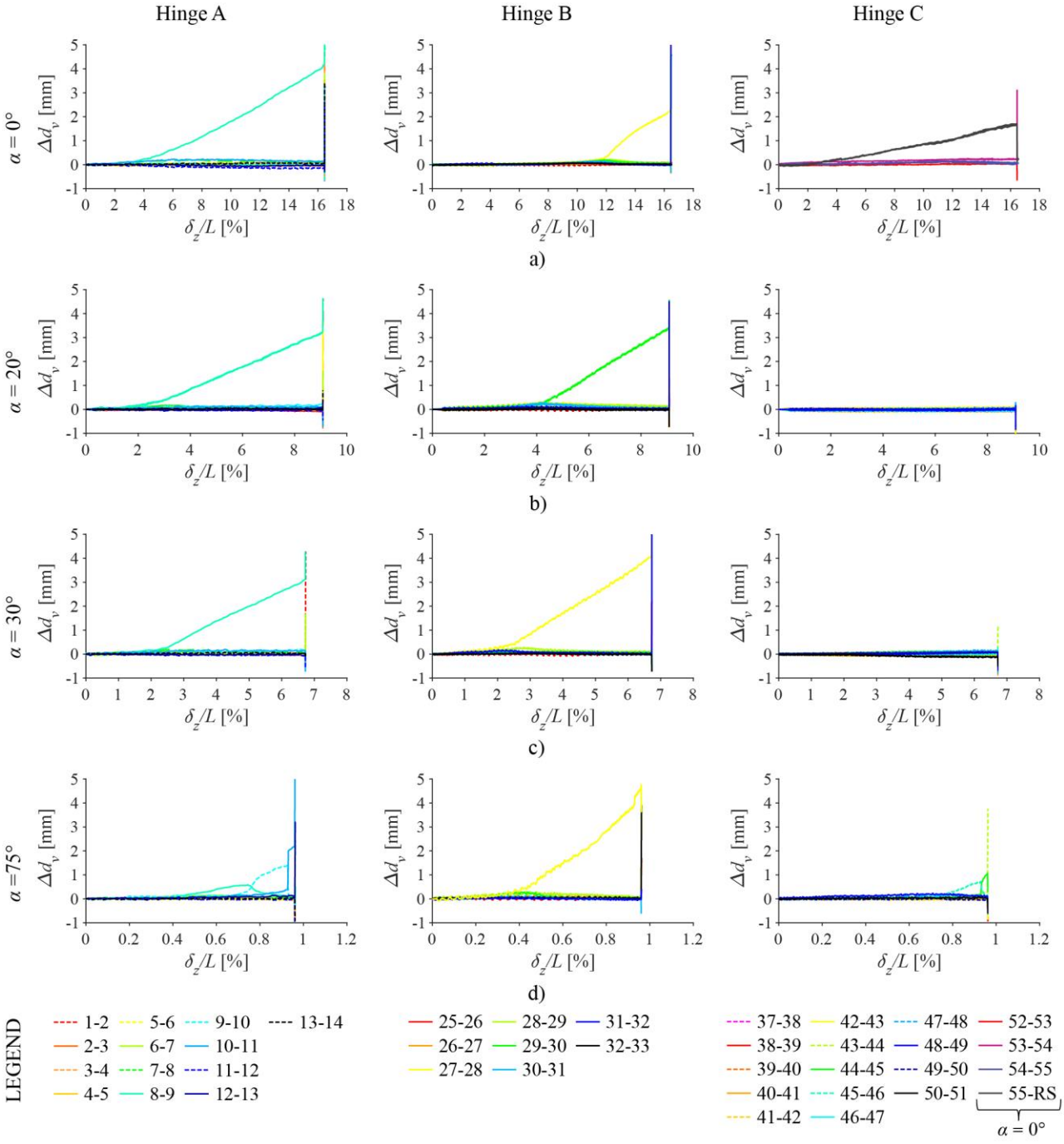

Fig. 18 Opening of hinges A (left), B (middle) and C (right) detected by plotting the change in the distance between markers of adjacent voussoirs, Δd_v, versus the normalized vertical displacement, δ_z/L: a) $\alpha = 0°$, b) $\alpha = 20°$, c) $\alpha = 30°$, d) $\alpha = 75°$ (see Fig. 16b for the identification of the voussoirs under study).

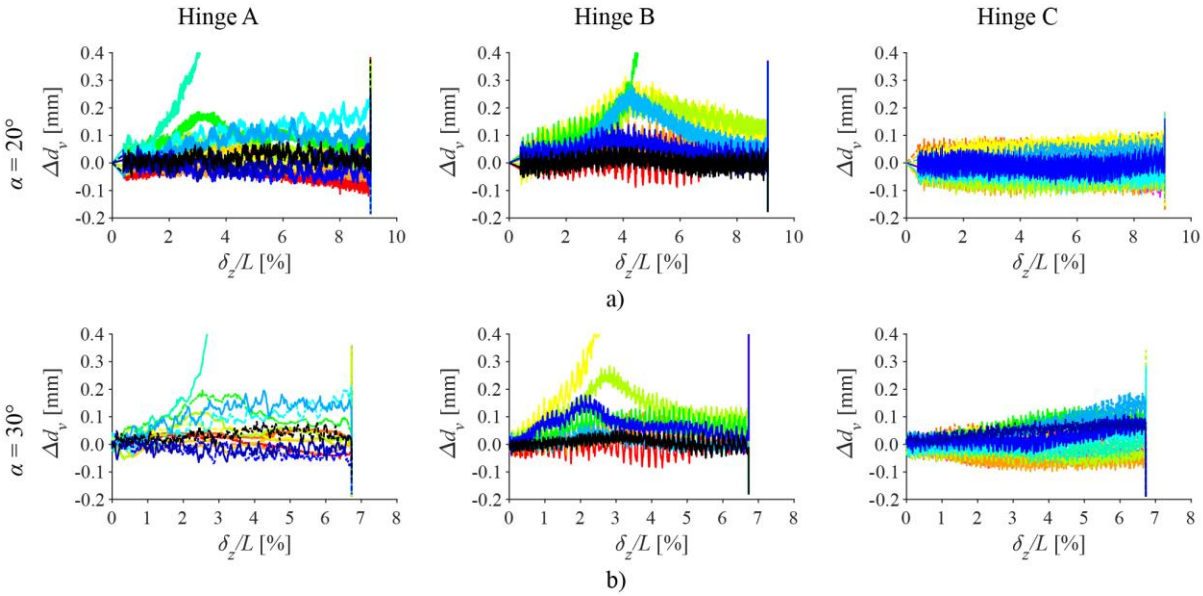

Fig. 19 Enlarged view of the y-axis of Fig. 18b-c (from -0.2 to 0.4): a) $\alpha = 20°$, b) $\alpha = 30°$.

4.1.3. Interpretation

The results from graphic statics together with the analysis of the evolution of the voussoir's displacements provided a full understanding of the arch response from the opening of the three initial hinges to collapse for every value of α investigated. In particular, in the cases in which, at collapse, only three hinges could be detected from the test recordings and the thrust line touched the arch external boundary only in three points (i.e., for α between 20° and 30°), the mobility needed to develop the collapse mechanism was found to be provided by the occurrence of very minor and distributed openings at a further section of the arch (right haunch at the intrados). These distributed openings allowed the downward rotation of block B-C to occur and, thus, had the same effect as a hinge in the activation of the collapse mechanism. It is important to note that, in a rigid-no tension arch coherent with Heyman's assumptions, collapse would require the opening of four or five fully developed hinges, that is, the thrust line at collapse should be tangent to the arch boundary in at least four points [43]. Since the voussoirs of the arch can be considered rigid and infinitely resistant in compression and sliding did not occur, the deviation from the behaviour of a rigid-no tension as well as the occurrence of minor and distributed openings can be reasonably attributed to the presence of small geometrical imperfections in the contact surfaces between adjacent voussoirs. These imperfections, which are unavoidable in any hand-made physical model and can result from the manufacturing process of the arch voussoirs, can also explain

the occurrence of minor and distributed openings in the early stages of the experimental tests (see Section 4.1.2).

The formation of minor distributed openings instead of a fully developed hinge at the intrados at the right haunch for some specific directions of imposed displacement can be ascribed to the abovementioned imperfections as well as to the different geometry of the arch deformed configuration obtained when varying α. For α between 20° and 30°, the downward rotation of block B-C was very small, and thus minor and distributed openings were sufficient to provide the arch with the mobility needed to activate collapse. In contrast, when α increased, the rotation became larger, requiring a fully developed hinge at the intrados. This explains why the thrust line moved closer to the intrados as α increased between 20° and 30° and also justifies why the distributed openings can be considered equivalent to a hinge.

In light of the foregoing considerations and combining the results obtained in terms of evolution of voussoirs' displacements with the failure modes observed in the tests, three different *modes* of evolution of the hinge configuration were identified when varying α:

- *Mode I* (for α between 0° and 15°). The three initial hinges followed the sequences I-E-E (from the fixed support) for every value of imposed displacement and did not generally move as support displacements increased. Collapse occurred by an asymmetrical four-hinge mechanism when a further hinge opened at the left support at the extrados (sequence E-I-E-E).
- *Mode II* (for α equal to 20°). The three initial hinges A, B and C were initially located according to the sequence I-E-E. As support displacements increased, hinge C closed at the extrados (right support) and opened (in the form of minor and distributed openings) at the intrados (right haunch). As a result, failure was governed by an asymmetrical four-hinge collapse mechanism with hinges located in the sequence E-I-E-I.
- *Mode III* (for α between 25° and 90°). Hinges A, B and C alternated between the intrados and the extrados (sequence I-E-I) for every value of imposed displacement. According to the value of α considered, either minor and distributed openings or fully developed hinges occurred at the

right haunch at the intrados. The intrados hinges A and C generally moved upwards towards the crown as the right support moved. For values of α up to 75°, collapse was governed by an asymmetrical four-hinge mechanisms with hinge located according to the sequence E-I-E-I. For α equal to 90°, the arch collapsed by an almost symmetrical five-hinge mechanism with two hinges occurring at the springings (sequence E-I-E-I-E).

The experimental results also showed that, as α increased, the arch response gradually evolved from that obtained in case of purely vertical displacements (α = 0°) to that obtained in the case of purely horizontal displacements (α = 90°). For α up to 15°, the evolution of the hinge configuration was the same as for α = 0°, indicating that the arch behaviour was governed by the vertical component δ_z of the imposed displacement. In contrast, for α between 25° and 75°, the evolution of the hinge configuration was the same as for α = 90° and, therefore, the arch response was driven by the horizonal component δ_x. For α equal to 20°, a transition between modes *I* and *III* occurred, since the initial and final hinge configurations were governed by the vertical (δ_z) and horizontal (δ_x) components of the imposed displacement, respectively. As expected, the final hinge configuration at collapse also became more symmetrical as α approached 90°: hinge B opened closer to the keystone and the position of the intrados hinges A and B became more symmetrical with respect to the vertical axis of symmetry of the arch.

4.2. Support reaction-displacement curves and limit displacement domain

For three representative angles α (0°, 30° and 90°), Fig. 20 and Fig. 21 show plots of the normalized horizontal (R_x/W) and vertical (R_z/W) reactions at the left (fixed) and right (moving) supports of the arch versus the normalized imposed displacement (vertical one for α = 0° and 30°, and horizontal one for α = 90°).

For every value of α, the horizontal support reaction-displacement curves are nonlinear (Fig. 20a-b on the left and Fig. 21a). As the imposed displacement increases, at both supports the horizontal reaction R_x first decreases and then substantially increases until it suddenly drops. This abrupt decrease, also observed in the case of the vertical reactions, indicates collapse. To explain this trend, it should be noted that, according to past numerical studies [13,35], the initial decrease in the horizontal support reaction

is produced by the opening of the three initial hinges. The drop is abrupt and occurs as soon the arch starts to move in the case of rigid models [13], while it is gradual and continues up to full development of the three initial hinges in the case of (FE) models provided with some elasticity [35]. A similar conclusion can be drawn for the arch tested in this work, though hinges initially appeared in the form of minor and distributed openings. Indeed, comparing the support reaction-displacement curves with the evolution of the distance between consecutive voussoirs (see, for example, Fig. 18a and Fig. 19b for α equal to 0° and 30°, respectively), it can be seen that all the three initial hinges have started or start to open in correspondence of the value of imposed displacement for which the horizontal reaction R_x reaches its minimum. The subsequent increase in the horizontal reaction can be attributed to the gradual changes in the geometry occurring as support displacements increase. The jumps in the curves (see Fig. 21a) are due to the movement of the intrados hinges from one voussoir to the next.

As shown in Fig. 20a-b (on the right) and Fig. 21b, the curves of the vertical reaction R_z at the two supports are specular, as should be expected. For every α between 0° and 75°, the curves are nonlinear. The vertical reaction at the right support slightly decreases at the early stages of the experimental tests and then increases up to collapse. Correspondingly, the vertical reaction at the left support initially slightly increases and then substantially decreases. As α increases, the change in the vertical reactions as well as their initial decrease/increase become less important. For α equal to 90°, the vertical reactions remain almost constant as the right support moves (Fig. 21b).

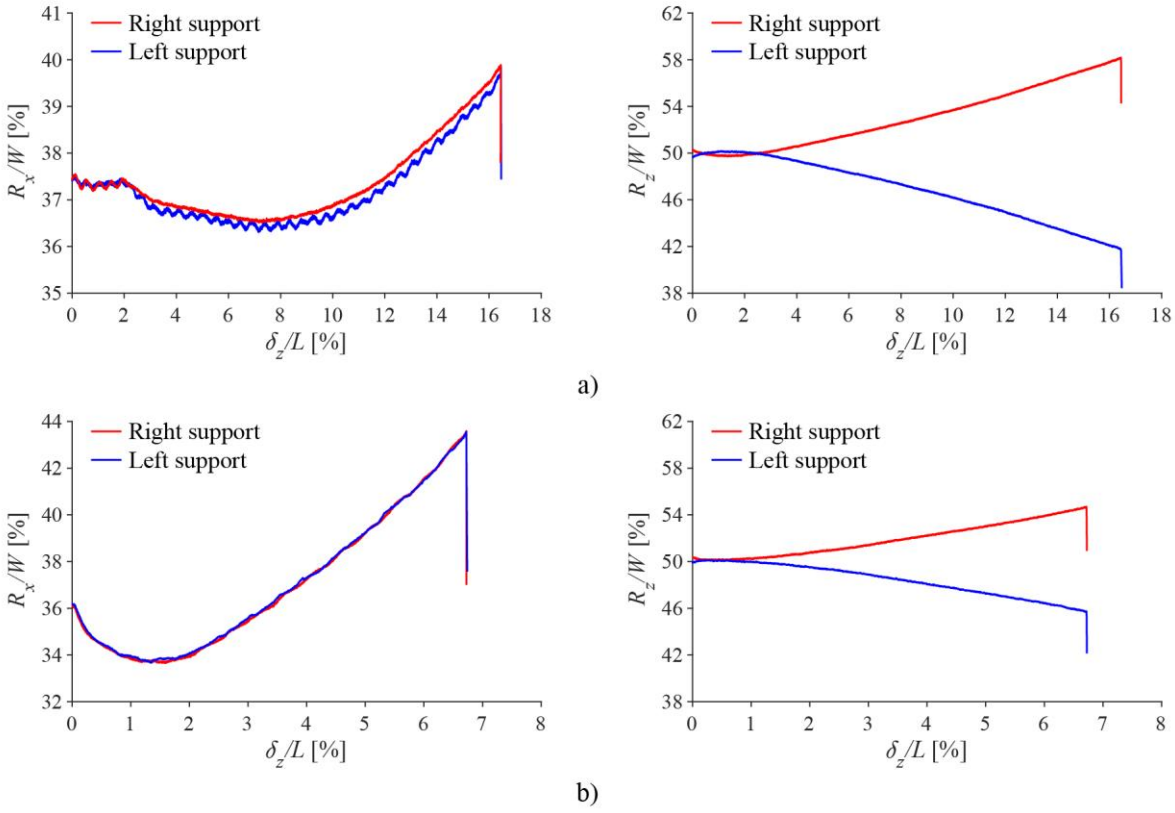

Fig. 20 Support reaction-displacement curves at the right and left supports for α = 0° (a), and α = 30° (b). On the left: normalized horizontal support reaction R_x/W vs. normalized vertical displacement δ_z/L; on the right: normalized vertical support reaction R_z/W vs. normalized vertical displacement δ_z/L.

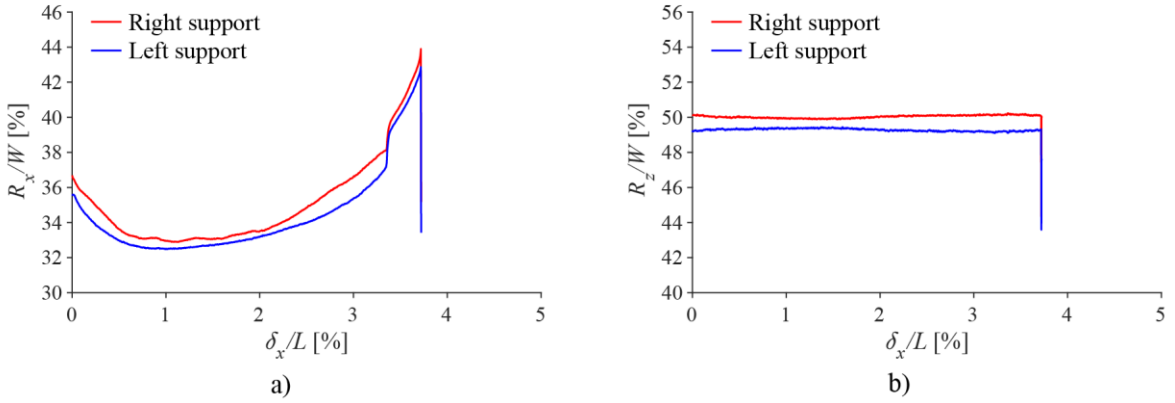

Fig. 21 Support reaction-displacement curves at the right and left supports for α = 90°: a) normalized horizontal support reaction R_x/W vs. normalized horizontal displacement δ_x/L, b) normalized vertical support reaction R_z/W vs. normalized horizontal displacement δ_x/L.

Fig. 22 depicts the support reaction-displacement curves obtained at the right support for all the values of α investigated. Purely vertical and horizontal support displacements were found to be limit conditions for the arch since all the curves corresponding to inclined displacements (i.e., α between 5° and 75°) are included between the curves for α equal to 0° and 90°. As expected, as α increases, the curves of both

the horizontal and vertical reactions approach the curve obtained for α equal to 90°. Conversely, as α decreases, the curves become more similar to the curve obtained for α equal to 0°. Looking at Fig. 22, it is also interesting to note that both the vertical and horizontal support reactions exhibit a very similar overall trend with the increase of support displacements no matter the *mode* of evolution of the hinge configuration experienced by the arch when varying α.

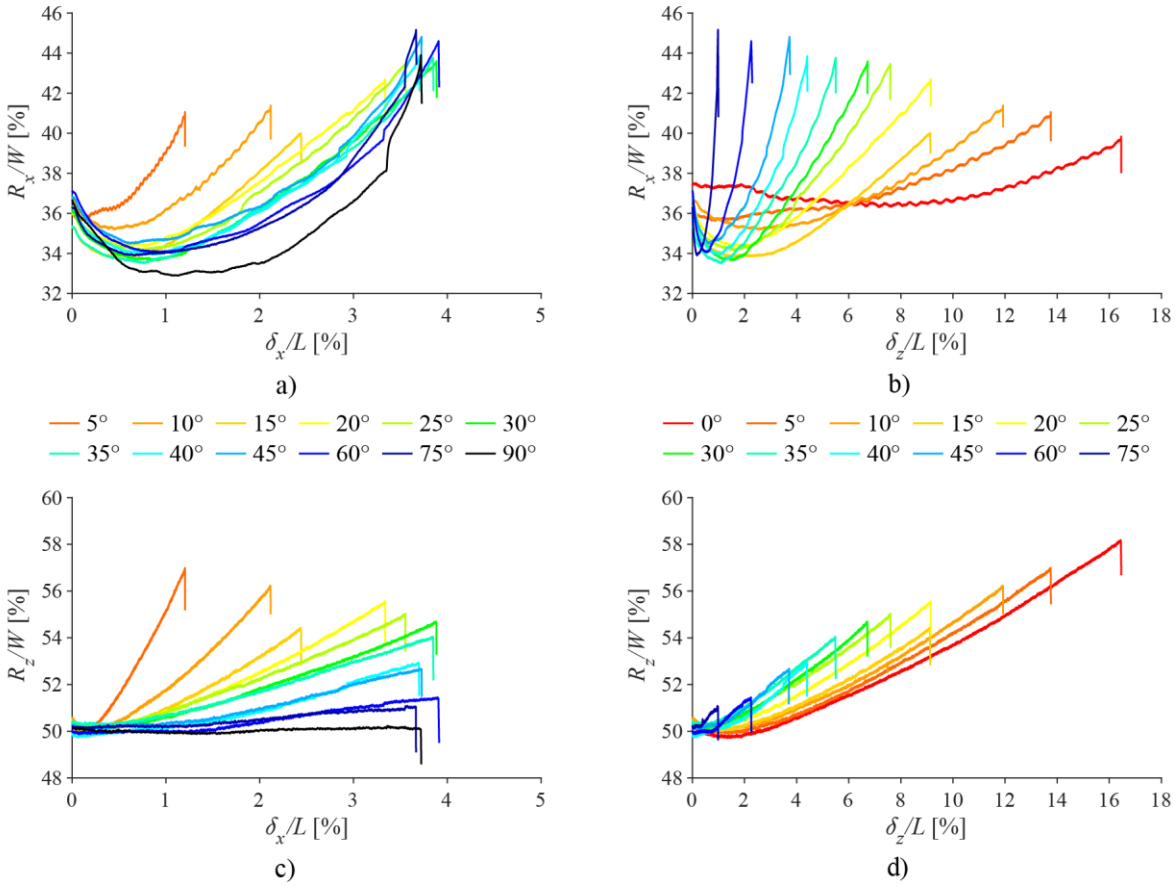

Fig. 22 Support reaction-displacement curves at the right support when varying α: a) curves normalized horizontal reaction R_x/W vs. normalized horizontal displacement δ_x/L, b) curves normalized horizontal reaction R_x/W vs. normalized vertical displacement δ_z/L, c) curves normalized vertical reaction R_z/W vs. normalized horizontal displacement δ_x/L, b) curves normalized vertical reaction R_z/W vs. normalized vertical displacement δ_z/L.

Fig. 23 reports the values of the normalized support reactions and displacements obtained at collapse when varying α between 0° and 90°. As Fig. 23a shows, as the angle α increases, the vertical collapse displacement decreases, dropping from about 16.5% of the arch span length for α equal to 0° to about 1.0% of the arch span length for α equal to 75°. The decrease is monotonic except between 15° and 20°, where there is almost no variation. This change in the trend can be attributed to the transition from *mode I* to *mode II*, which also affects the vertical support reaction at collapse. As shown in Fig. 23c, indeed,

at the right support, $R_{z,u}/L$ decreases monotonically with increasing α except between 15° and 20°, where it increases abruptly. As expected, an opposite trend is obtained at the left support.

As can be seen in Fig. 23b, the horizontal collapse displacement significantly increases with increasing α up to 30°. Beyond this value, it remains almost constant and ranges approximately between 3.7% and 3.9% of the arch span length. Similarly, at both supports, the horizontal reaction at collapse exhibits a more significant growth up to 25° (Fig. 23d). An abrupt decrease, however, occurs between 10° and 15°.

According to the results reported in Fig. 23a-b, it can be concluded that the arch has a significantly larger capacity to withstand vertical support displacements compared to horizontal displacements. Indeed, the vertical and horizontal collapse displacements obtained for α equal to 0° and 90° are equal to about 16.5% and 3.7% of the arch span length, respectively.

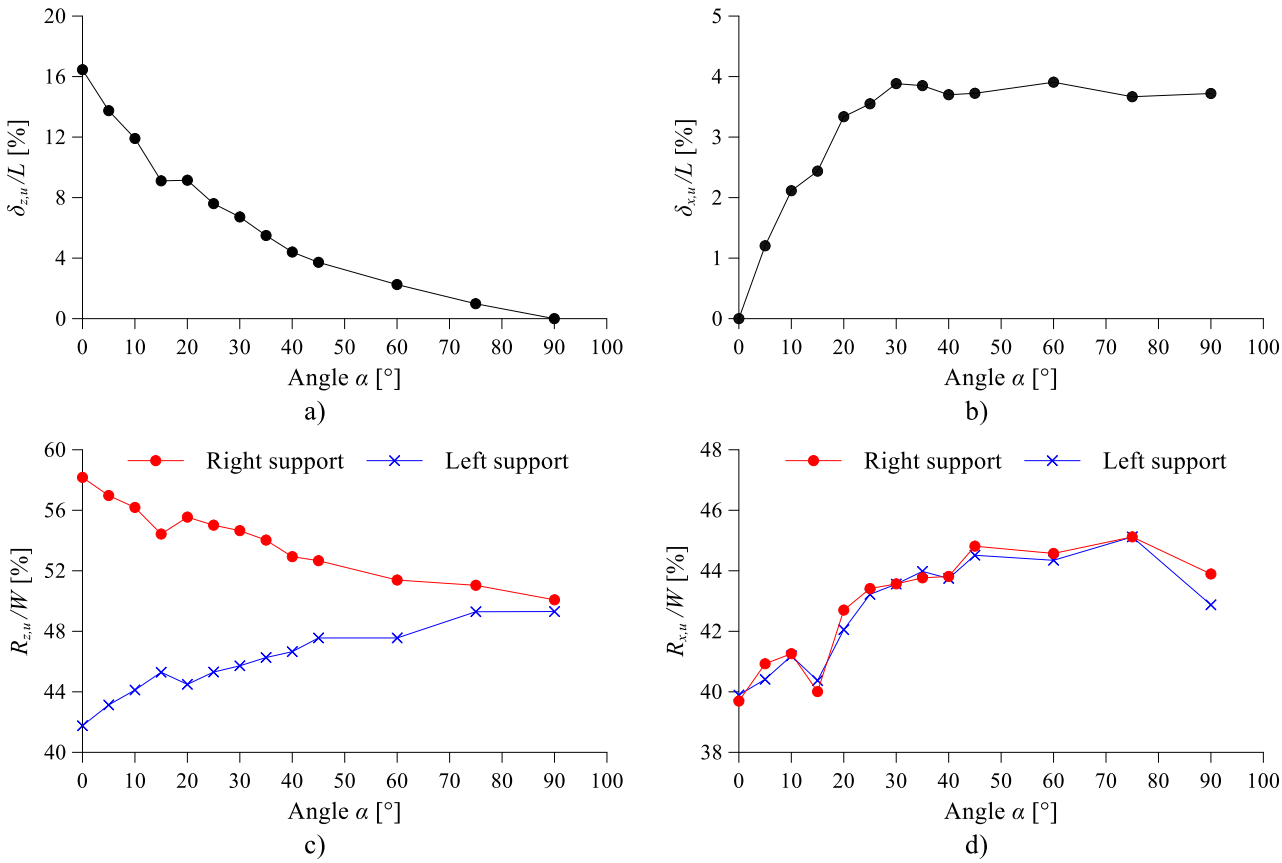

Fig. 23 Collapse displacements and support reactions at collapse for α between 0° and 90°: a) normalized vertical collapse displacement $\delta_{z,u}/L$, b) normalized horizontal collapse displacement $\delta_{x,u}/L$, c) normalized vertical support reactions at collapse $R_{z,u}/W$, d) normalized horizontal support reactions at collapse $R_{x,u}/W$.

Fig. 24 presents the limit displacement domain of the tested arch, which was obtained by plotting the normalized vertical collapse displacement $\delta_{z,u}/L$ versus the normalized horizontal collapse displacement $\delta_{x,u}/L$ for every value of α. Different trends can be recognized, which reflect the *modes* of evolution of the hinge configuration identified in Section 4.1. For α between 0° and 15°, as α increases, the vertical collapse displacement decreases, whereas the horizontal one increases. This trend can be associated to *mode I*. The relation between vertical and horizontal collapse displacements is almost linear up to $\alpha = 10°$. The abrupt decrease in $\delta_{z,u}/L$ observed for α equal to 15º can be explained considering that hinges do not change position for α between 0° and 10°, whereas for α equal to 15° hinge A moves by one voussoir towards the crown, causing collapse to occur for a significantly lower value of imposed displacement.

When α increases from 15° to 20° and the transition between *mode I* and *mode II* occurs, the vertical collapse displacement does not change, while the horizontal one increases by about 1%.

For larger angles, corresponding to *mode III* ($\alpha = 25° \div 90°$), the vertical collapse displacement decreases significantly with the increase in α, whereas the horizontal collapse displacement changes only slightly, ranging between 3.5% and 3.9% of the arch span length for every value of α.

What clearly emerges from Fig. 24 is that both *modes I and III* took place in a specific range of α, while *mode II* was detected for α = 20° only. This result is strictly related to the values of α considered in this work. If further displacement directions were investigated between 15° and 25°, *mode II* could be found to occur for further values of α close to 20°. Indeed, as already mentioned in this section and the previous one, the arch response gradually changed from the one for α = 0° to the one for α = 90°.

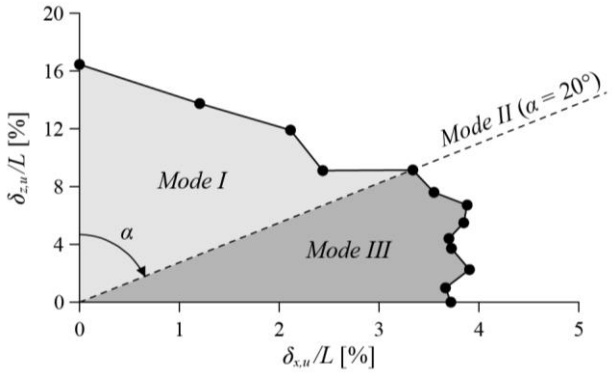

Fig. 24 Limit displacement domain of the tested arch.

4.3. Repeatability

As described in Section 3, the experimental tests were repeated seven times for α equal to 0° and 90°. The results in terms of hinge position and collapse displacements are reported in Table 4 and Table 5. As done in Table 3, the joints where hinges appear are numbered from left to right, being joint no.1 the joint at the left support.

For α equal to 0° (Table 4), failure was always governed by an asymmetrical four-hinge mechanism. The hinge position and collapse displacement results were generally repeatable. In six of the seven tests, all the four hinges were located at the same position and the collapse displacement ranged between 15.7% and 16.5% of the arch span length. Only in test #2, hinge A appeared closer to the crown by one voussoir and the collapse displacement decreased to 14.4% of the arch span length, showing that the displacement capacity was strictly related to the position of hinge A. In any case, considering all the tests, the standard deviation of the normalized collapse displacement was equal to only 0.7%.

In the case of α equal to 90° (Table 5), the final position at collapse of hinge C was the same in all the tests, while the positions of hinges A and B slightly varied. As anticipated in Section 4.1, depending on the test, collapse involved the opening of four or five hinges and the location of hinges A and C was symmetrical or asymmetrical with respect to the vertical axis of symmetry of the arch. However, the collapse displacement was only slightly affected by these differences in the hinge position and type of failure mode. As shown in Table 5, indeed, it ranged between 3.6% and 3.8% of the arch span length in all the tests. The average value was equal to 3.7% with a very low standard deviation of 0.07%.

Table 4 Hinge position at collapse and normalized vertical collapse displacement for α equal to 0°.

Test id #	Joint no.				$\delta_{z,u}/L$ [%]
	Hinge A	Hinge B	Hinge C	Hinge D	
1	9-I	28-E	56-E	1-E	16.1
2	10-I	28-E	56-E	1-E	14.4
3	9-I	28-E	56-E	1-E	16.1
4	9-I	28-E	56-E	1-E	16.0
5	9-I	28-E	56-E	1-E	16.1
6	9-I	28-E	56-E	1-E	15.7
7	9-I	28-E	56-E	1-E	16.5
				Mean value	15.8
				Standard deviation	0.7

Table 5 Hinge position at collapse and normalized horizontal collapse displacement for α equal to 90°.

Test id #	Joint no.					$\delta_{x,u}/L$ [%]
	Hinge A	Hinge B	Hinge C	Hinge D	Hinge E	
1	11-I	27-E	45-I	1-E	56-E	3.8
2	12-I	30-E	45-I	1-E	56-E	3.6
3	12-I	28-E	45-I	1-E	56-E	3.7
4	12-I	28-E	45-I	1-E	-	3.6
5	11-I	28-E	45-I	1-E	-	3.7
6	11-I	29-E	45-I	1-E	56-E	3.6
7	11-I	28-E	45-I	1-E	56-E	3.6
					Mean value	3.7
					Standard deviation	0.07

In light of the results obtained for α equal to 0° and 90°, repeatable results are expected to occur also for the other values of α investigated in this work.

5. Conclusions

This paper investigates the response of masonry arches to large support displacements by performing a set of experimental tests on a 1:10 small-scale model of a segmental arch built as a dry-joint assembly of bicomponent composite voussoirs. As main novelty of the work, the arch was tested to collapse under thirteen combinations of vertical and horizontal support displacements. For purely vertical and horizontal displacements, the tests were repeated seven times, showing highly repeatable results in terms of both collapse mechanisms and ultimate displacement capacity. Such repeatability demonstrated the

ability of the experimental set-up to investigate the arch stability without any significant influence by the construction and assemblage of the physical model.

Provided that the collapse mechanisms were coherent with the ones identified so far in the literature, new conclusions about the arch response to inclined support displacements were drawn. As a major result, the direction of the imposed support displacements (expressed with the angle α measured from the vertical) was found to significantly affect the arch behaviour in terms of collapse mechanism, evolution of the arch deformed configuration, support reaction-displacement curves, ultimate displacement capacity and support reactions at collapse. The response of the arch was also observed to gradually change from the response obtained for purely vertical displacements to the response obtained for purely horizontal ones as α increased from 0° to 90°.

For the first time in the literature, three *modes* of evolution of the hinge configuration with increasing support displacements were identified experimentally when varying the direction of the imposed displacements. The identification of these *modes* helps in the understanding of the damage experienced by masonry arches in historic structures. By knowing the hinge position as a function of the direction of support displacements, the causes of damage can indeed be identified more easily. Phenomena like subsidence and foundation settlements on one side and leaning of the supporting piers or buttresses on the other side are expected to produce the same crack patterns obtained in the case of purely vertical and horizontal support displacements, respectively. Conversely, the combination of the above-mentioned phenomena as well as landslides will result in the same damage patterns induced by inclined support displacements.

A limit displacement domain, expressed as a function of the angle α, was also proposed. This domain provides useful information about the ultimate displacement capacity of the tested arch and indicates the combinations of vertical and horizontal displacements that cause collapse to occur.

As a final comment, it is worth noting that, although the mockup was built in such a way that it complied with Heyman's assumptions on the behaviour of the masonry material, the arch did not to behave as a perfectly rigid-no tension structure. Three hinges did not immediately appear when support displacements were imposed, but the arch accommodated the initial changes in the geometry by forming

minor and distributed openings in consecutive joints. Furthermore, the activation of the collapse mechanism did not always require the opening of four or five fully developed hinges, as would occur in rigid no-tension arches. For some specific values of α, due to the geometry of the arch deformed configuration, three fully developed hinges together with minor and distributed openings at a further section of the arch profile were found to be sufficient for collapse to occur. Since the arch voussoirs can be considered rigid and infinitely resistant in compression and sliding did not occur, the deviation from the behaviour of a rigid-no tension arch was attributed to the imperfections in the contact surfaces between adjacent voussoirs. Future works will be devoted to investigating the role of the joints in the response of masonry arches to large support displacements.

Future research will also assess if the results obtained in this work for a specific case study can be extended to a broader range of arched structures, such as arches with a different geometry and number of voussoirs. No matter the arch shape and discretization in voussoirs, the same *modes* of evolution of the hinge configuration identified in this study are expected to occur, at least for circular arches, for which the same final hinge configurations obtained in this work for purely vertical and horizontal displacements were observed to occur in the literature. Nevertheless, also in this case, the presence of minor and distributed openings should be thoroughly verified. In the arch under study, minor and distributed openings could easily occur due to the arch segmental shape and small size of the voussoirs, which led the thrust line to pass very close to the arch profile in correspondence to several consecutive joints. A different response can be, however, expected if the voussoirs are significantly larger in width and the arch has a different shape.

Fundings

The financial support of PRIN 2015 Program by the Italian Ministry of Education, University and Research (MIUR) is gratefully acknowledged for funding the research project “Protecting the Cultural Heritage from water-soil interaction related threats” (Prot. No. 2015EAM9S5), which is the main framework of the study presented in this article.

References

[1] Ochsendorf JA. The masonry arch on spreading supports. Struct Eng 2006;84(2):29–35.

[2] Ferrero C. Structural behaviour of masonry arches on moving supports: from on-site observation to experimental and numerical analysis. PhD diss., University of Genoa-Technical University of Catalonia; 2021.

[3] Ochsendorf JA. Collapse of masonry structure. PhD diss., University of Cambridge; 2002.

[4] Smars P. Kinematic stability of masonry arches. Adv Mater Res 2010;133:429–34.

[5] Romano A. Modelling, analysis and testing of masonry structures. PhD diss., University of Naples Federico II; 2005.

[6] Romano A, Ochsendorf JA. The mechanics of gothic masonry arches. Int J Arch Heritage 2010;4(1):59–82, https://doi.org/10.1080/15583050902914660.

[7] Zampieri P, Faleschini F, Zanini MA, Simoncello N. Collapse mechanisms of masonry arches with settled springing. Eng Struct 2018;156:363–74, https://doi.org/10.1016/ j.engstruct.2017.11.048.

[8] Zampieri P, Simoncello N, Pellegrino C. Structural behaviour of masonry arch with no-horizontal springing settlement. Frattura ed Integrità Strutturale 2018;12(3):182–190, https://doi.org/10.3221/IGF-ESIS.43.14.

[9] Zampieri P, Cavalagli N, Gusella V, Pellegrino C. Collapse displacements of masonry arch with geometrical uncertainties on spreading supports. Comput Struct 2018;208:118-129, https://doi.org/10.1016/j.compstruc.2018.07.001.

[10] Alforno M, Venuti F, Calderini C. Validation of Simplified Micro-models for the Static Analysis of Masonry Arches and Vaults. Int J Archit Herit 2020, https://doi.org/10.1080/15583058.2020.1808911.

[11] Masciotta M-G, Pellegrini D, Girardi M, Padovani C, Barontini A, Lourenço PB, Brigante D, Fabbrocino G. Dynamic characterization of progressively damaged segmental masonry arches with one settled support: experimental and numerical. Frattura ed Integrità Strutturale 2020;51:423-441, https://doi.org/10.3221/IGF-ESIS.51.31.

[12] Ferrero C, Rossi M, Calderini C, Roca P. Experimental and numerical analysis of a scaled dry-joint arch on moving supports. Int J Mason Res Innov 2021;6(4), https://doi.org/10.1504/IJMRI.2021.10035577.

[13] Iannuzzo A, Dell'Endice A, Van Mele T, Block P. Numerical limit analysis-based modelling of masonry structures subjected to large displacements. Comput Struct 2021; 242, https://doi.org/10.1016/j.compstruc.2020.106372.

[14] Galassi S, Misseri G, Rovero L, Tempesta G. Failure modes prediction of masonry voussoir arches on moving supports. Eng Struct 2018;173:706-717, https://doi.org/10.1016/j.engstruct.2018.07.015

[15] Galassi S, Misseri G, Rovero L, Tempesta G. Analysis of Masonry Pointed Arches on Moving Supports: A Numeric Predictive Model and Experimental Evaluations. In: Proc. of XXIV AIMETA Conference 2019, 15-19 September 2019, Rome, Italy, p- 1-21.

[16] Portioli FP, Cascini L. Large displacement analysis of dry-jointed masonry structures subjected to settlements using rigid block modelling. Eng Struct 2017; 148:485-496, https://doi.org/10.1016/j.engstruct.2017.06.073

[17] Galassi S, Misseri G, Rovero. Capacity assessment of masonry arches on moving supports in large displacements: Numerical model and experimental validation. Eng Fail Anal 2021;129, https://doi.org/10.1016/j.engfailanal.2021.105700

[18] Barentin C, Van Mele T, Block, P. Robotically controlled scale-model testing of masonry vault collapse. Meccanica 2017; 53:1917–1929, https://doi.org/10.1007/s11012-017-0762-6.

[19] D'Altri AM, De Miranda S, Castellazzi G, Sarhosis V, Hudson J, Theodossopoulos D. (2020) Historic barrel vaults undergoing differential settlements. Int J Archit Herit 2020;14(8): 1196-1209, https://doi.org/10.1080/15583058.2019.1596332.

[20] Foti D, Vacca V, Facchini I. DEM modeling and experimental analysis of the static behavior of a dry-joints masonry cross vaults. Constr Build Mater 2018;170:111–120, https://doi.org/10.1016/j.conbuildmat.2018.02.202.

[21] Torres B, Bertolesi E, Moragues JJ, Calderón PA, Adam JM. A full-scale timbrel cross vault subjected to vertical cyclical displacements in one of its supports. Eng Struct 2019; 183: 791–804, https://doi.org/10.1016/j.engstruct.2019.01.054.

[22] Torres B, Bertolesi E, Moragues JJ, Calderón PA, Adam JM. Experimental investigation of a full-scale timbrel masonry cross vault subjected to vertical settlement. Constr Build Mater 2019; 221: 421–432, https://doi.org/10.1016/j.conbuildmat.2019.06.015.

[23] Rossi M, Calvo Barentin , Van Mele, T, Block P. Experimental study on the behaviour of masonry pavilion vaults on spreading supports. Structures 2017;11:110-120, https://doi.org/10.1016/j.istruc.2017.04.008.

[24] Van Mele T, McInerney J, DeJong M, Block P. Physical and computational discrete modelling of masonry vault collapse. In: Proc. of 8th international conference on Structural Analysis of Historical Constructions (SAHC2012), 15–17 October 2012, Wroclaw, Poland, p. 2552–60.

[25] Bertolesi E, Torres B, Adam JM, Calderón PA, Moragues JJ. Effectiveness of Textile Reinforced Mortar (TRM) materials for the repair of full-scale timbrel masonry cross vaults. Eng Struct 2020:220, https://doi.org/10.1016/j.engstruct.2020.110978.

[26] Quinonez A, Zessin J, Nutzel A, Ochsendorf JA. Small-Scale Models for Testing Masonry Structures. Adv Mater Res 2010;133-134:497-502, https://doi.org/10.4028/www.scientific.net/AMR.133-134.497.

[27] Verstrynge E, Schueremans L, Smars P, Van Gemert. 2007 D. Design and testing of masonry arches: a project of bachelor students in civil engineering. In: Proceedings of the International Conference on Arch Bridges (ARCH'07), 2007, p. 351-358.

[28] Heyman J. The stone skeleton. Cambridge University Press; 1995.

[29] Theodossopoulos D. Structural behaviour of historic masonry cross vaults. PhD diss., University of Edinburgh; 2001.

[30] Theodossopoulos, D, Sinha BP, Usmani AS, Macdonald AJ. Assessment of the structural response of masonry cross vaults. Strain 2002;38(3):119–27, https://doi.org/10.1046/j.0039-2103.2002.00021.x.

[31] Zessin J, Lau W, Ochsendorf JA. Equilibrium of cracked masonry domes. Proc Inst Civ Eng: Eng Comput Mech 2010;163(EM3):135–145.

[32] Shapiro E.E. Collapse mechanism of small-scale unreinforced masonry vaults. M.S. thesis in Building Technology, Massachusetts Institute of Technology; 2012.

[33] Pippard AJS, Ashby R. An experimental study of the voussoir arch. J Inst Civ Eng 1939;10(3): 383-404.

[34] Ferrero C, Cambiaggi L, Vecchiattini R, Calderini C. Damage assessment of historic masonry churches exposed to slow-moving. Int J Archit Herit 2021;15(8): 1170-1195, https://doi.org/10.1080/15583058.2020.1799259.

[35] Ferrero C, Calderini C, Portioli FP, Roca P. Large displacement analysis of dry-joint masonry arches subject to inclined support movements. Eng Struct 2021; 238.

[36] Prochima. Plastoforma PL; Technical data sheet. 2019. Accessed July 14, 2019. https://www.prochima.it/files/PLASTOFORMA-PL_versione-6.pdf.

[37] Heyman J. The stone skeleton. Int J Solids Struct 1966;2(2):249–79.

[38] SANYO DENKI. SanMotion F2 - 2-Phase stepping systems; Technical data sheet. 2020 Accessed December 13, 2020. https://products.sanyodenki.com/en/sanmotion/stepping/f2/.

[39] Lunghi F, Pavese A, Peloso S, Lanese I, Silvestri D. Computer Vision System for Monitoring of Dynamic Structural Testing. In: Fardis MN, Rakicevic ZT, editors. Role of Seismic Testing Facilities in Performance-Based Earthquake Engineering. Springer; 2012, p. 159-176.

[40] Heyman J. The masonry arch. Ellis Horwood Ltd; 1982.

[41] Huerta S. The analysis of masonry architecture: A historical approach. Arch Sci Rev 2011;51(4):297–328.

[42] Roca P, Cervera M, Gariup G, Pela L. Structural analysis of masonry historical constructions. Classical and advanced approaches. Arch Comput Methods Eng 2010;17:299–325, https://doi.org/10.1007/s11831-010-9046-1.

[43] Heyman J. The safety of masonry arches. Int. J. Mech. Sci 1969;11(4):363–385.